



NRL/MR/6790--93-7365

2

Nonlinear Thomson Scattering of Intense Laser Pulses from Beams and Plasmas

ERIC ESAREY
PHILLIP SPRANGLE

*Beam Physics Branch
Plasma Physics Division*

DTIC
ELECTE
SEP 22 1993
S A D

SALLY K. RIDE

*California Space Institute
University of California
San Diego, La Jolla, CA*

August 23, 1993

Approved for public release; distribution unlimited.

93-21945



SSP8

93 9 21 000

REPORT DOCUMENTATION PAGE

Form Approved
OMB No. 0704-0188

Public reporting burden for this collection of information is estimated to average 1 hour per response, including the time for reviewing instructions, searching existing data sources, gathering and maintaining the data needed, and completing and reviewing the collection of information. Send comments regarding this burden estimate or any other aspect of this collection of information, including suggestions for reducing this burden, to Washington Headquarters Services, Directorate for Information Operations and Reports, 1215 Jefferson Davis Highway, Suite 1204, Arlington, VA 22202-4302, and to the Office of Management and Budget, Paperwork Reduction Project (0704-0188), Washington, DC 20503.

1. AGENCY USE ONLY (Leave Blank)	2. REPORT DATE <p style="text-align: center;">August 23, 1993</p>	3. REPORT TYPE AND DATES COVERED	
4. TITLE AND SUBTITLE <p style="text-align: center;">Nonlinear Thomson Scattering of Intense Laser Pulses from Beams and Plasmas</p>		5. FUNDING NUMBERS <p style="text-align: center;">DOE Contract # DOE-AI05-83ER40117</p>	
6. AUTHOR(S) <p style="text-align: center;">Eric Esarey, Sally K. Ride* and Phillip Sprangle</p>		8. PERFORMING ORGANIZATION REPORT NUMBER <p style="text-align: center;">NRL/MR/6790-93-7365</p>	
7. PERFORMING ORGANIZATION NAME(S) AND ADDRESS(ES) <p style="text-align: center;">Naval Research Laboratory Washington, DC 20375-5320</p>		10. SPONSORING/MONITORING AGENCY REPORT NUMBER	
9. SPONSORING/MONITORING AGENCY NAME(S) AND ADDRESS(ES) <p style="text-align: center;">Department of Energy Washington, DC 20375-5320</p>		11. SUPPLEMENTARY NOTES <p style="text-align: center;">*California Space Institute, University of California, San Diego, La Jolla, CA</p>	
12a. DISTRIBUTION/AVAILABILITY STATEMENT <p style="text-align: center;">Approved for public release; distribution unlimited.</p>		12b. DISTRIBUTION CODE	
13. ABSTRACT (<i>Maximum 200 words</i>) <p>A Comprehensive theory is developed to describe the nonlinear Thomson scattering of intense laser fields from beams and plasmas. This theory is valid for linearly or circularly polarized incident laser fields of arbitrary intensities and for electrons of arbitrary energies. Explicit expressions for the intensity distributions of the scattered radiation are calculated and numerically evaluated. The space-charge electrostatic potential, which is important in high density plasmas and prevents the axial drift of electrons, is included self-consistently. Various properties of the scattered radiation are examined, including the linewidth, angular distribution, and the behavior of the radiation spectra at ultrahigh intensities. Non-ideal effects, such as electron energy spread and beam emittance, are discussed. A laser synchrotron source (LSS), based on nonlinear Thomson scattering, may provide a practical method for generating tunable, near monochromatic, well collimated, short pulse x-rays in a compact, relatively inexpensive source. Two examples of possible LSS configurations are presented: an electron beam LSS generating hard (30 keV, 0.4 Å) x-rays and a plasma LSS generating soft (0.3 keV, 40 Å) x-rays. These LSS configurations are capable of generating ultrashort (~1 ps) x-ray pulses with high peak flux ($\geq 10^{21}$ photons/s) and brightness ($\geq 10^{19}$ photons/s-mm²-mrad² 0.1% BW).</p>			
14. SUBJECT TERMS <p style="text-align: center;">Synchrotron radiation Thomson scattering Laser-plasma interactions</p>		15. NUMBER OF PAGES <p style="text-align: center;">59</p>	
17. SECURITY CLASSIFICATION OF REPORT <p style="text-align: center;">UNCLASSIFIED</p>		16. PRICE CODE	
18. SECURITY CLASSIFICATION OF THIS PAGE <p style="text-align: center;">UNCLASSIFIED</p>		20. LIMITATION OF ABSTRACT <p style="text-align: center;">UL</p>	
19. SECURITY CLASSIFICATION OF ABSTRACT <p style="text-align: center;">UNCLASSIFIED</p>		20. LIMITATION OF ABSTRACT <p style="text-align: center;">UL</p>	

CONTENTS

I.	Introduction	1
II.	Election Motion in Intense Laser Fields	6
III.	Scattered Radiation	12
	A. Linear Polarization	13
	B. Circular Polarization	16
IV.	Radiation Properties	20
	A. Radiated Power	20
	B. Resonance Function	21
	C. Ultra-Intense Behavior	22
V.	Non-Ideal Effects	28
	A. Electron Energy Spread	28
	B. Electron Beam Energy Loss	29
	C. Ponderomotive Density Depletion	29
	D. Plasma Dispersion	30
VI.	Laser Synchrotron Sources	32
	A. Electron-Beam LSS	32
	B. Plasma LSS	34
VII.	Conclusion	37
	Acknowledgments	39
	References	40
	Table I	42
	Table II	43

DTIC QUALITY INSPECTED 1

Accession For	
NTIS	<input checked="" type="checkbox"/>
CRA&I	<input checked="" type="checkbox"/>
DTIC TAB	<input type="checkbox"/>
Unannounced	<input type="checkbox"/>
Justification	
By	
Distribution /	
Availability Codes	
Dist	Avail and/or Special
A-1	

NONLINEAR THOMSON SCATTERING OF INTENSE LASER PULSES FROM BEAMS AND PLASMAS

I. INTRODUCTION

The development of a compact source of bright, near monochromatic, well collimated, short pulse x-rays would have profound wide ranging applications in a number of areas. These areas include x-ray spectroscopy, microscopy and radiography, medical and biological imaging, x-ray analysis of ultrafast processes, and x-ray holography. One method for producing such an x-ray beam is by the nonlinear Thomson scattering of intense laser pulses from electron beams and plasmas [1-9]. Current methods of x-ray production include third generation synchrotron sources, which are based on high energy electron storage rings and undulator magnetic fields [10-17]. Alternatively, x-rays can be produced by a laser synchrotron source (LSS), based on nonlinear Thomson scattering, in which the magnetic undulator is replaced by ultrahigh intensity laser pulses and the electron storage ring is replaced by a compact electron accelerator of substantially lower energy or by a stationary plasma [5-7]. The compactness of the LSS makes it an attractive alternative, particularly at high x-ray energies (> 10 keV), where conventional synchrotrons require very high energy (> 5 GeV) storage rings. To generate high peak fluxes of x-rays in an LSS, ultra-intense laser pulses are necessary. Recent advances in compact, solid-state, short pulse lasers based on the method of chirped-pulse amplification [18-20], provide the technology for generating the ultrahigh laser intensities required by an LSS.

In the following, a comprehensive theory is developed to describe the nonlinear Thomson scattering of intense laser fields from beams and plasmas. This theory is valid for linearly or circularly polarized incident laser fields of arbitrary intensities and for electrons of arbitrary energies. Explicit expressions for the intensity distributions of the scattered radiation are calculated and numerically evaluated. The effects of the space-charge electrostatic potential are included self-consistently and non-ideal effects, such as electron energy spread and beam emittance, are discussed. These results are then applied to possible LSS configurations.

An LSS [5-7], using either an electron beam or a plasma, potentially has a number of

Manuscript approved July 2, 1993.

attractive features: (i) tunable and near-monochromatic x-rays can be obtained over the entire x-ray spectrum (from ultraviolet to gamma-rays), (ii) the x-rays can be produced in ultrashort pulses (~ 1 ps), (iii) a much lower electron beam energy (~ 300 times less) is needed to produce a given photon energy than in conventional synchrotrons, (iv) the device can be compact and inexpensive compared to conventional synchrotrons, (v) much higher energy photons ($\gtrsim 30$ keV) can be produced than in conventional synchrotrons, (vi) the bandwidth can be small ($\sim 1\%$) and is not limited by the length of the undulator as in conventional synchrotrons, (vii) consequently, narrow bandwidth x-rays can be obtained with long coherence lengths, (viii) the x-ray polarization is easily adjusted by changing the incident laser polarization, and (ix) high peak photon flux and brightness can be obtained using current technology. The capability of the LSS in yielding high average fluxes and brightnesses is currently limited by the repetition rates of high intensity laser systems.

An important parameter in the discussion of LSS radiation/Thomson scattering is the dimensionless laser strength parameter, a_0 , which is analogous to the undulator strength parameter, K , frequently used in conventional synchrotron radiation literature. The laser strength parameter is the normalized amplitude of the vector potential of the incident laser field, $a_0 = eA_0/m_e c^2$, and is related to the laser intensity, I_0 , and power, P_0 , by

$$a_0 = 0.85 \times 10^{-9} \lambda_0 [\mu\text{m}] I_0^{1/2} [\text{W}/\text{cm}^2] \quad (1)$$

and $P_0[\text{GW}] = 21.5(a_0 r_0/\lambda_0)^2$, where λ_0 is the wavelength and r_0 is the spot size of the laser (a Gaussian transverse profile is assumed). When $a_0 \ll 1$, Thomson scattering occurs in the linear regime and radiation is generated at the fundamental frequency, $\omega = \omega_1$. When $a_0 \gtrsim 1$, Thomson scattering occurs in the nonlinear regime and radiation is generated at harmonics in addition to the fundamental, i.e., $\omega = \omega_n = n\omega_1$, where $n = 1, 2, 3, \dots$ is the harmonic number. Compact laser systems based on chirped-pulse amplification can deliver modest energy ($\gtrsim 10$ J), ultrashort ($\lesssim 1$ ps) laser pulses at ultrahigh powers ($\gtrsim 10$ TW) and intensities ($\gtrsim 10^{18}$ W/cm²). For $\lambda_0 \sim 1$ μm , $a_0 \gtrsim 1$ requires $I_0 \gtrsim 10^{18}$ W/cm². Hence, laser systems which can be used to experimentally explore Thomson scattering in the nonlinear regime currently exist. Furthermore, these powers and intensities are sufficient to produce ultrashort LSS x-ray pulses with high peak fluxes and brightnesses.

In the LSS, two avenues exist for generating short wavelength radiation. The first is to exploit the relativistic doppler factor which arises from backscattering laser radiation from a counterstreaming relativistic electron beam. In this case, the wavelength of the fundamental ($n = 1$) backscattered radiation along the axis is given by $\bar{\lambda} = \lambda_0 \gamma_{\perp}^2 / [(1 + \beta_0) \gamma_0]^2$, where $\gamma_0 = (1 - \beta_0^2)^{-1/2}$ is the initial relativistic factor of the electron beam (prior to the laser interaction), $\beta_0 = v_0/c$ is the initial normalized electron velocity and $\gamma_{\perp} = (1 + a_0^2/2)^{1/2}$. Hence, for $\gamma_0 \gg 1$ and $a_0^2 \ll 1$, $\bar{\lambda} \simeq \lambda_0/4\gamma_0^2$ and extremely short wavelength radiation can be generated. In practical units, the photon energy, $E_p = \hbar\bar{\omega}$, and wavelength, $\bar{\lambda}$, of the fundamental backscattered radiation are given by

$$E_p[\text{keV}] = \frac{0.019 E_b^2[\text{MeV}]}{(1 + a_0^2/2) \lambda_0[\mu\text{m}]}, \quad (2a)$$

$$\bar{\lambda}[\text{\AA}] = 650 \lambda_0[\mu\text{m}] \frac{(1 + a_0^2/2)}{E_b^2[\text{MeV}]}, \quad (2b)$$

where E_b is the electron beam energy and $\gamma_0^2 \gg 1$ has been assumed. For a conventional synchrotron source [9-16] using a undulator magnet, $\bar{\lambda} = \lambda_u/2\gamma_0^2$, or $E_p[\text{keV}] = 0.95 E_b^2[\text{GeV}]/\lambda_u[\text{cm}]$ and $\bar{\lambda}[\text{\AA}] = 13.0 \lambda_u[\text{cm}]/E_b^2[\text{GeV}]$, where λ_u is the undulator magnet wavelength and $K^2 \ll 1$ and $\gamma_0^2 \gg 1$ have been assumed. Since the laser wavelength in the LSS ($\lambda_0 \sim 1 \mu\text{m}$) is more than four orders of magnitude shorter than the wavelength of a conventional undulator magnet ($\lambda_u \gtrsim 4 \text{ cm}$), a much lower energy electron beam (~ 300 times less) can be used in the LSS to produce a given photon energy. Hence, compared to a conventional storage-ring based synchrotron, the LSS can be a compact, inexpensive device, particularly at high photon energies ($E_p > 10 \text{ keV}$). As an example, consider synchrotron sources producing 30 keV photons ($\lambda = 0.40 \text{ \AA}$), assuming $a_0^2 \ll 1$ and $K^2 \ll 1$. In a conventional synchrotron using a $\lambda_u = 4 \text{ cm}$ undulator period, electron beam energies of $E_b \geq 12 \text{ GeV}$ are needed. In the LSS using a $\lambda_0 = 1 \mu\text{m}$ laser, $E_b = 40 \text{ MeV}$, which is typical of the energies available from compact accelerators, such as rf linacs or betatrons.

The second avenue to short wavelengths is to exploit the harmonic frequency upshift factor, $\lambda = \lambda_1/n$, where λ_1 is the wavelength of the fundamental. For $a_0^2 \gg 1$, numerous harmonics are generated. The result is a near-continuum of scattered radiation with harmonics extending out to some critical harmonic number, $n_c \sim a_0^3$, beyond which the

intensity of the scattered radiation rapidly decreases. Hence, an ultra-intense laser incident on a stationary plasma ($\gamma_0 = 1$) can generate short wavelength radiation, $\lambda = \lambda_0/n$. The critical photon energy for a plasma-based LSS is given by

$$E_p[\text{eV}] = 1.24n_c/\lambda_0[\mu\text{m}], \quad (3)$$

where $n_c \sim a_0^3$. Assuming laser technology limits $a_0 \lesssim 10$ and $\lambda_0 \sim 1 \mu\text{m}$ implies that the scattered radiation is limited to $\lambda \gtrsim 10 \text{ \AA}$ and $E_p \lesssim 1 \text{ keV}$. Hence, a plasma-based LSS is limited by present laser technology to the soft to medium x-ray regime.

Tunability of the LSS radiation can be achieved by adjusting either the electron energy or the laser intensity, as indicated by Eqs. (2) and (3). Neglecting thermal effects, it can be shown that the linewidth of the scattered radiation for a particular n harmonic of frequency ω_n is given by $\Delta\omega/\omega_n = 1/nN_0$, where N_0 is the number of laser periods with which the electron interacts. In principle, since N_0 is typically large ($N_0 \gtrsim 300$), narrow linewidth x-rays can be generated. In practice, the linewidth will be limited by thermal effects. For example, the normalized energy spread associated with an electron beam, $\Delta E/E_b$, limits the linewidth to $\Delta\omega/\omega_n \simeq 2\Delta E/E_b$. An additional advantage of generating LSS radiation using an electron beam is that the scattered radiation is well collimated about the backscattered direction (i.e., the direction of the electron beam). For an electron beam with $\gamma_0 \gg 1$ and $a_0 < 1$, the backscattered radiation with linewidth $\Delta\omega/\omega \simeq 1/N_0$ is confined to a radiation cone of half-angle $\theta \simeq 1/(\gamma_0\sqrt{N_0})$. For a plasma with $a_0 > 1$, the radiation is scattered over a much larger angle. When $a_0 \gg 1$, numerous harmonics are generated, and tunability is achieved by filtering the scattered radiation. An additional advantage in using a plasma is that very high electron densities can be achieved in comparison to densities obtainable in electron beams. The scattered power, as well as photon flux and brightness, scale linearly with density, hence, the use of high electron densities is favored.

Thomson scattering theory is a classical description which is valid provided the scattered photon energy is small compared to the electron energy, i.e., $\hbar\omega \ll \gamma_0 m_e c^2$. For a plasma, this implies photon energies less than 500 keV. For an electron beam with $\gamma_0 \gg 1$, $\lambda_0 = 1 \mu\text{m}$ and $a_0 < 1$, this implies $\gamma_0 < 10^5$, i.e., electron beam energies less than 50 GeV. Nonlinear Thomson scattering of intense radiation from a single electron initially

at rest was examined analytically in considerable detail in the classic work of Sarachik and Schappert [1]. (This work was recently reexamined by Castillo-Herrera and Johnston [9].) However, the important effects of the space charge potential [2,21], which arises in high density plasmas, was neglected and scattering from electron beams was not discussed. Waltz and Manley [2] also discussed Thomson scattering from plasmas and pointed out that the space charge potential was important in preventing the drift of electrons in the direction of the incident laser. However, explicit expressions for the scattered intensity distribution for arbitrary a_0 were not calculated and scattering from electron beams was not considered. Many authors [10-17] have analyzed the production of synchrotron radiation in the interaction of relativistic electron beams with static magnetic undulator and wiggler fields, a process which is somewhat similar to Thomson scattering. These analyses require that $K/\gamma_0 \ll 1$ (analogous to $a_0/\gamma_0 \ll 1$), an assumption which need not be made in the analysis of nonlinear Thomson scattering. In this paper, nonlinear Thomson scattering of intense laser fields from electron beams and from plasmas is examined analytically and numerically. This analysis is valid for linearly and circularly polarized incident laser fields of arbitrary intensities and for electron beams of arbitrary energies (up to the limits of classical theory). The effects of the space-charge potential are included self-consistently and various non-ideal effects, such as electron energy spread, are discussed.

The remainder of this paper is organized as follows. In Sect. II, the orbits of electrons in intense laser fields, both linearly and circularly polarized, are calculated including the effects of the self-consistent electrostatic potential. Explicit expressions for the scattered intensity distributions are derived in Sect. III. These are general expressions, valid for electron beams and plasmas, and for arbitrary laser intensities. Properties of the scattered radiation are examined in Sect. IV, including a calculation of the total power radiated from an electron beam or a plasma, an examination of the resonance function and the behavior of the radiation spectra in the ultra-intense regime, i.e., $a_0^2 \gg 1$. Various non-ideal effects are discussed in Sect. V, including the effects of electron energy spread, electron beam energy loss, ponderomotive density depletion and plasma dispersion. These results are applied to possible LSS configurations in Sect. VI, and specific examples of an electron-beam LSS and a plasma LSS are presented. Section VII is the conclusion.

II. ELECTRON MOTION IN INTENSE LASER FIELDS

The laser field and space charge field of the electrons can be represented using the normalized vector and scalar potentials, $\mathbf{a} = e\mathbf{A}/m_e c^2$ and $\hat{\Phi} = e\Phi/m_e c^2$, respectively, where m_e is the electron mass and e is the magnitude of the electron charge. In the Coulomb gauge, $\nabla \cdot \mathbf{a} = 0$ implies $a_z = 0$ in one-dimension (1D). Then, \mathbf{a}_\perp represents the laser field and $\hat{\Phi}$ represents the space-charge field of the plasma. The normalized vector potential of a laser of arbitrary polarization is represented by

$$\mathbf{a} = (a_0/\sqrt{2}) \left[(1 + \delta_p)^{1/2} \cos k_0 \eta \mathbf{e}_x + (1 - \delta_p)^{1/2} \sin k_0 \eta \mathbf{e}_y \right], \quad (4)$$

where $k_0 = 2\pi/\lambda_0$ is the wavenumber of the laser field, $\eta = z + ct$, $\delta_p = 1$ for linear polarization and $\delta_p = 0$ for circular polarization. Using this representation, $(a^2)_s = a_0^2/2$ for both linear and circular polarizations, where the subscript s signifies the slow component (an averaging over the laser wavelength). Hence, the average laser power $P_0 \sim (a^2)_s$ is constant for a given value of a_0 , independent of polarization, i.e., $P_0[\text{GW}] = 21.5(a_0 r_0/\lambda_0)^2$, assuming a Gaussian transverse profile of the form $|a| \sim \exp(-r^2/r_0^2)$. In the following, the laser field is assumed to be moving to the left ($-z$ direction) and the electrons are initially (prior to the interaction with the laser field) moving to the right ($+z$ direction) with an initial axial velocity $v_z = v_0$ (see Fig. 1).

The electron motion in the fields \mathbf{a} and $\hat{\Phi}$ is governed by the relativistic Lorentz equation, which may be written in the form

$$\frac{1}{c} \frac{d}{dt} \mathbf{u} = \nabla \hat{\Phi} + \frac{1}{c} \frac{\partial}{\partial t} \mathbf{a} - \boldsymbol{\beta} \times (\nabla \times \mathbf{a}), \quad (5)$$

where $\boldsymbol{\beta} = \mathbf{v}/c$ is the normalized electron velocity, $\mathbf{u} = \mathbf{p}/m_e c = \gamma \boldsymbol{\beta}$ is the normalized electron momentum, and $\gamma = (1 + u^2)^{1/2} = (1 - \beta^2)^{-1/2}$ is the relativistic factor. Assuming that the laser field, \mathbf{a}_\perp , and hence the quantities $\hat{\Phi}$, $\boldsymbol{\beta}$, \mathbf{u} , and γ , are functions only of the variable $\eta = z + ct$, Eq. (5) implies the existence of two constants of the motion [21,22],

$$\frac{d}{d\eta} (\mathbf{u}_\perp - \mathbf{a}_\perp) = 0, \quad (6a)$$

$$\frac{d}{d\eta} (\gamma + u_z - \hat{\Phi}) = 0. \quad (6b)$$

Equation (6a) is conservation of canonical transverse momentum in 1D, and Eq. (6b) can be interpreted as conservation of energy in the wave frame. Equations (6a) and (6b) can be integrated to give [21,22]

$$\mathbf{u}_\perp = \mathbf{a}_\perp, \quad (7a)$$

$$\gamma + u_z - \hat{\Phi} = \gamma_0(1 + \beta_0), \quad (7b)$$

where, prior to the laser interaction ($\mathbf{a}_\perp = 0$), $\mathbf{u}_\perp = \hat{\Phi} = 0$, $\gamma = \gamma_0$ and $u_z = \gamma_0\beta_0$ have been assumed. The two constants of the motion, Eqs. (7a) and (7b), completely describe the nonlinear motion of electrons in the potentials \mathbf{a} and $\hat{\Phi}$. They allow the electron motion to be specified solely in terms of the fields, i.e.,

$$\beta_z = \frac{h_0^2 - (1 + a^2)}{h_0^2 + (1 + a^2)}, \quad (8a)$$

$$\gamma = (h_0^2 + 1 + a^2)/2h_0, \quad (8b)$$

$$\beta_\perp = \mathbf{a}_\perp/\gamma, \quad (8c)$$

where $h_0 = \gamma_0(1 + \beta_0) + \hat{\Phi}$.

The self-consistent space-charge potential of the electrons, $\hat{\Phi}$, can be determined using the continuity equation and Poisson's equation,

$$\frac{1}{c} \frac{\partial}{\partial t} n_e + \nabla \cdot (n_e \boldsymbol{\beta}) = 0, \quad (9a)$$

$$\nabla^2 \hat{\Phi} = k_p^2 (n_e/n_0 - 1), \quad (9b)$$

where n_e is the electron density, $k_p = \omega_p/c$, $\omega_p = (4\pi e^2 n_0/m_e)^{1/2}$ is the plasma frequency and n_0 is the ambient density. Equation (9b) assumes that the initial equilibrium (prior to the laser pulse) space-charge potential, $\hat{\Phi}^{(0)}$, is negligible. For a plasma, a neutralizing background of stationary ions is assumed, i.e., $\hat{\Phi}^{(0)} = 0$. For a long, uniform electron beam of radius r_b , $|\hat{\Phi}^{(0)}| \lesssim k_p^2 r_b^2/4 = \nu_b$, where $\nu_b = I_b/I_{b0}$ is the Budker parameter, I_b is the beam current, and $I_{b0}[\text{kA}] = 17\beta_z$. Since $\nu_b \ll 1$ for beams of interest, $\hat{\Phi}^{(0)}$ can be neglected. Assuming $n_e = n_e(\eta)$, Eq. (9a) implies [21,22]

$$\frac{d}{d\eta} [n_e(1 + \beta_z)] = 0, \quad (10)$$

hence, $n_e = n_0(1 + \beta_0)/(1 + \beta_z)$. Substituting this result into Eq. (9b) and using Eq. (8a) give [21,22]

$$\frac{d^2}{d\eta^2}\Psi = \frac{\hat{k}_p^2}{2} \left[\frac{(1 + a^2)}{(1 + \Psi)^2} - 1 \right], \quad (11)$$

where $\Psi = \hat{\Phi}/\gamma_0(1 + \beta_0)$ and $\hat{k}_p = k_p/\gamma_0^{3/2}(1 + \beta_0)$.

Equation (11) describes the self-consistent electrostatic potential induced by the interaction of the laser field. The solution for Ψ is, in general, highly nonlinear. Simple solutions can be obtained in two limits in which the characteristic temporal variation of the laser envelope, τ_L (typically the laser rise time), is compared to an effective plasma period, $(c\hat{k}_p)^{-1}$. In the short-pulse limit, $\tau_L \ll (c\hat{k}_p)^{-1}$, Eq. (11) implies $|\Psi| \ll 1$ provided $a_0 < 2/c\tau_L\hat{k}_p$, where a_0 is the amplitude of the laser pulse, e.g., $a = a_0 \cos k_0\eta$. In the long pulse limit, $\tau_L \gg (c\hat{k}_p)^{-1}$, the left side of Eq. (11) can be neglected and it can be shown that $\Psi \simeq (1 + a^2)_s^{1/2} - 1$, where the subscript s signifies the slow part. Throughout the following, the quantity $(1 + a^2)_s^{1/2} \simeq (1 + a_0^2/2)^{1/2}$ will be approximated as nearly constant, i.e., $|d(a^2)_s/d\eta| \ll k_0(a^2)_s$, which implies that $L_0 \gg \lambda_0$, where $L_0 = c\tau_L$ is the length of the laser envelope.

For applications which utilize intense lasers with pulse lengths $\tau_L \sim 1$ ps, the short-pulse limit is relevant to interactions with electron beams as long as the beam density is sufficiently low, $n_0/\gamma_0^3 \ll 10^{16} \text{ cm}^{-3}$. On the other hand, the long-pulse limit is relevant to interactions with stationary ($\gamma_0 = 1$) plasmas as long as the density is sufficiently high, $n_0 \gg 10^{16} \text{ cm}^{-3}$. Under these conditions, the parameter $h_0 = \gamma_0(1 + \beta_0)(1 + \Psi)$ is given by

$$h_0 = \begin{cases} \gamma_0(1 + \beta_0), & \text{e-beam (short pulse),} \\ (1 + a_0^2/2)^{1/2}, & \text{plasma (long pulse).} \end{cases} \quad (12)$$

Notice that in the limit of a low-density plasma with $n_0 \ll 10^{16}$, $|\hat{\Phi}| \ll 1$ and $h_0 \simeq 1$. This corresponds to the single particle limit considered in Ref. [1].

The electron orbits, $\mathbf{r}(\eta) = x \mathbf{e}_x + y \mathbf{e}_y + z \mathbf{e}_z$, can be calculated as a function of η using Eqs. (8a-c) and the relation

$$\frac{1}{c} \frac{d\mathbf{r}}{dt} = \boldsymbol{\beta} = (1 + \beta_z) \frac{d\mathbf{r}}{d\eta}, \quad (13)$$

which gives $dr/d\eta = \mathbf{u}/h_0$. For a linearly polarized laser of the form given by Eq. (4) with $\delta_p = 1$, the electron orbits are given by

$$u_x = a_0 \cos k_0\eta, \quad (14a)$$

$$u_y = 0, \quad (14b)$$

$$u_z = [h_0^2 - (1 + a_0^2 \cos^2 k_0\eta)] / 2h_0. \quad (14c)$$

Hence,

$$x(\eta) = x_0 + r_1 \sin k_0\eta, \quad (15a)$$

$$y(\eta) = y_0, \quad (15b)$$

$$z(\eta) = z_0 + \beta_1\eta + z_1 \sin 2k_0\eta, \quad (15c)$$

where additional terms of order λ_0/L_0 have been neglected and

$$r_1 = a_0/h_0k_0, \quad (16a)$$

$$z_1 = -a_0^2/8h_0^2k_0, \quad (16b)$$

$$\beta_1 = (1 - 1/M_0) / 2, \quad (16c)$$

with $M_0 = h_0^2/(1 + a_0^2/2)$, i.e.,

$$M_0 = \begin{cases} \gamma_0^2(1 + \beta_0)^2/(1 + a_0^2/2), & \text{e-beam,} \\ 1, & \text{plasma.} \end{cases} \quad (17)$$

Similarly, for a circular polarized laser ($\delta_p = 0$), the electron orbits are given by

$$u_x = (a_0/\sqrt{2}) \cos k_0\eta, \quad (18a)$$

$$u_y = (a_0/\sqrt{2}) \sin k_0\eta, \quad (18b)$$

$$u_z = [h_0^2 - (1 + a_0^2/2)] / 2h_0. \quad (18c)$$

Hence,

$$x(\eta) = x_0 + (r_1/\sqrt{2}) \sin k_0\eta, \quad (19a)$$

$$y(\eta) = y_0 - (r_1/\sqrt{2}) \cos k_0\eta, \quad (19b)$$

$$z(\eta) = z_0 + \beta_1\eta, \quad (19c)$$

where, again, additional terms of order λ_0/L_0 have been neglected. In the above equations, (x_0, y_0, z_0) are related to the initial position of the electron.

The axial drift velocity of the electrons, $\bar{\beta}_z$, can be written in terms of the parameter β_1 . Since $\eta = z + ct$, Eq. (19c) implies $z = (z_0 + \beta_1 ct)/(1 - \beta_1)$. Hence,

$$\bar{\beta}_z = \beta_1/(1 - \beta_1) = (M_0 - 1)/(M_0 + 1) \quad (20)$$

is the average normalized velocity of the electrons in the axial direction. Notice that in the dense plasma (long pulse) limit, $M_0 = 1$ and $\bar{\beta}_z = 0$. For a low density plasma in the single particle limit $M_0 = (1 + a_0^2/2)^{-1}$ and $\bar{\beta}_z = -(a_0^2/2)/(2 + a_0^2/2)$. Hence, in the single particle limit, a single electron initially at rest receives a finite average drift velocity due to the ponderomotive force associated with the rise of the incident laser pulse, as pointed out in Ref. [1]. For an electron in a dense plasma (long pulse limit), $\bar{\beta}_z = 0$ and there is no average axial motion of the electrons [2,21,22]. Physically, $\bar{\beta}_z = 0$ is achieved through a balance between the ponderomotive force and the space-charge force set up during the rise of the laser pulse.

The self-consistent electron density in the presence of the laser field can be calculated using the constant of motion $n_e(1 + \beta_z) = n_0(1 + \beta_0)$. This can be written in terms of the parameter h_0 as

$$n_e = n_0(1 + \beta_0)(h_0^2 + 1 + a^2)/2h_0^2. \quad (21)$$

Of particular interest is the slow part (η averaged) of the density, n_{es} . For a tenuous electron beam (short pulse limit), $h_0 = \gamma_0(1 + \beta_0)$ and $n_{es} \simeq 1$, assuming $h_0^2 \gg (1 + a_0^2/2)$. For a dense plasma (long pulse limit), $h_0 = (1 + a_0^2/2)^{1/2}$ and $n_{es} = 1$. However, this is not the case for a plasma in the single particle regime. For a tenuous plasma in the short pulse limit, $h_0 = 1$ and $n_{es} = n_0(1 + a_0^2/4)$. In this regime, the plasma density is enhanced due the ponderomotive force associated with the rise of the laser pulse and the resulting finite axial drift motion of the electrons, $\bar{\beta}_z$.

The above results have assumed the 1D limit, which is valid when $r_0 \gg \lambda_0$ and when the quiver motion is much greater than the ponderomotive motion. In three-dimensions (3D), the ponderomotive motion, $\delta \mathbf{u} = \mathbf{u} - \mathbf{a}$, is given [23] by $\partial \delta \mathbf{u} / \partial \eta = \nabla(\phi - \gamma)$. The quasi-static approximation implies that the quantity $\gamma + u_z - \phi - a_z$ is a constant of

the motion, which is the 3D generalization of Eq. (7b). For a plasma, it follows that $|\delta u|/|a| \lesssim \lambda_p a_0/r_0$, whereas for a relativistic electron beam, $|\delta u|/|a| \lesssim L_0 a_0/\gamma_0 r_0$. The ponderomotive motion can be neglected when $|\delta u|/|a| \ll 1$, which is true in the cases discussed below.

III. SCATTERED RADIATION

The energy spectrum of the radiation emitted by a single electron in an arbitrary orbit $\mathbf{r}(t)$ and $\boldsymbol{\beta}(t)$ can be calculated from the Lienard-Wiechert potentials [24],

$$\frac{d^2 I}{d\omega d\Omega} = \frac{e^2 \omega^2}{4\pi^2 c} \left| \int_{-T/2}^{T/2} dt [\mathbf{n} \times (\mathbf{n} \times \boldsymbol{\beta})] \exp[i\omega(t - \mathbf{n} \cdot \mathbf{r}/c)] \right|^2, \quad (22)$$

where $d^2 I/d\omega d\Omega$ is the energy radiated per frequency, ω , per solid angle, Ω , during the interaction time, T , and \mathbf{n} is a unit vector pointing in the direction of observation. Introducing the spherical coordinates (r, θ, ϕ) and unit vectors $(\mathbf{e}_r, \mathbf{e}_\theta, \mathbf{e}_\phi)$, where $x = r \sin \theta \cos \phi$, $y = r \sin \theta \sin \phi$, $z = r \cos \theta$, and

$$\mathbf{e}_r = \sin \theta \cos \phi \mathbf{e}_x + \sin \theta \sin \phi \mathbf{e}_y + \cos \theta \mathbf{e}_z, \quad (23a)$$

$$\mathbf{e}_\theta = \cos \theta \cos \phi \mathbf{e}_x + \cos \theta \sin \phi \mathbf{e}_y - \sin \theta \mathbf{e}_z, \quad (23b)$$

$$\mathbf{e}_\phi = -\sin \phi \mathbf{e}_x + \cos \phi \mathbf{e}_y, \quad (23c)$$

and by identifying $\mathbf{e}_r = \mathbf{n}$, give

$$\begin{aligned} \mathbf{n} \times (\mathbf{n} \times \boldsymbol{\beta}) &= -(\beta_x \cos \theta \cos \phi + \beta_y \cos \theta \sin \phi - \beta_z \sin \theta) \mathbf{e}_\theta \\ &\quad + (\beta_x \sin \phi - \beta_y \cos \phi) \mathbf{e}_\phi, \end{aligned} \quad (24a)$$

$$\mathbf{n} \cdot \mathbf{r} = x \sin \theta \cos \phi + y \sin \theta \sin \phi + z \cos \theta. \quad (24b)$$

The scattered radiation will be polarized in the direction of $\mathbf{n} \times (\mathbf{n} \times \boldsymbol{\beta})$. Hence, $I = I_\theta + I_\phi$, where I_θ and I_ϕ are the energies radiated with polarizations in the \mathbf{e}_θ and \mathbf{e}_ϕ directions, respectively. In terms of the independent variable $\eta = z + ct$,

$$\frac{d^2 I_\theta}{d\omega d\Omega} = \frac{e^2 \omega^2}{4\pi^2 c^3} \left| \int_{-\eta_0}^{\eta_0} d\eta \left(\frac{dx}{d\eta} \cos \theta \cos \phi + \frac{dy}{d\eta} \cos \theta \sin \phi - \frac{dz}{d\eta} \sin \theta \right) \exp(i\psi) \right|^2, \quad (25a)$$

$$\frac{d^2 I_\phi}{d\omega d\Omega} = \frac{e^2 \omega^2}{4\pi^2 c^3} \left| \int_{-\eta_0}^{\eta_0} d\eta \left(\frac{dx}{d\eta} \sin \phi - \frac{dy}{d\eta} \cos \phi \right) \exp(i\psi) \right|^2, \quad (25b)$$

where

$$\psi = k [\eta - z(1 + \cos \theta) - x \sin \theta \cos \phi - y \sin \theta \sin \phi], \quad (26)$$

$k = \omega/c$, $\eta_0 = L_0/2$, L_0 is the laser pulse length and $L_0 \gg \lambda_0 = 2\pi/k_0$ has been assumed. In deriving the above expressions, the relation $c\boldsymbol{\beta}dt = (d\mathbf{r}/d\eta)d\eta$ was used, where $\mathbf{r} = \mathbf{r}(\eta)$ is given by Eqs. (15) and (19).

A. Linear Polarization

The electron orbit for a linearly polarized incident laser field of the form given by Eq. (4) with $\delta_p = 1$ is given by Eq. (15). The phase ψ can be written as

$$\begin{aligned} \psi = & \psi_0 + [1 - \beta_1(1 + \cos \theta)] k\eta \\ & - (kr_1 \sin \theta \cos \phi) \sin k_0\eta - [kz_1(1 + \cos \theta)] \sin 2k_0\eta, \end{aligned} \quad (27a)$$

$$\psi_0 = -k [z_0(1 + \cos \theta) + x_0 \sin \theta \cos \phi + y_0 \sin \theta \sin \phi]. \quad (27b)$$

Using the Bessel identity

$$\exp(ib \sin \sigma) = \sum_{n=-\infty}^{\infty} J_n(b) \exp(in\sigma), \quad (28)$$

where J_n are Bessel functions, allows the phase factor $\exp [i(\psi + \ell k_0\eta)]$ to be written as

$$\exp [i(\psi + \ell k_0\eta)] = \sum_{m,n=-\infty}^{\infty} J_m(\hat{\alpha}_z) J_{n-2m+\ell}(\hat{\alpha}_x) \exp [i(\psi_0 + \bar{k}\eta)], \quad (29)$$

where

$$\bar{k} = k [1 - \beta_1(1 + \cos \theta)] - nk_0, \quad (30a)$$

$$\hat{\alpha}_z = kz_1(1 + \cos \theta), \quad (30b)$$

$$\hat{\alpha}_x = kr_1 \sin \theta \cos \phi. \quad (30c)$$

In order to evaluate Eqs. (25a) and (25b), it is necessary to evaluate the integrals

$$\hat{I}_{(x,y,z)} = \int_{-\eta_0}^{\eta_0} d\eta \frac{d(x,y,z)}{d\eta} \exp(i\psi). \quad (31)$$

Using the orbits, Eq. (15), along with the identities in Eqs. (28) and (29),

$$\hat{I}_x = k_0 r_1 e^{i\psi_0} \sum_{m,n=-\infty}^{\infty} \left(\frac{\sin \bar{k}\eta}{\bar{k}} \right) J_m(\hat{\alpha}_z) [J_{n-2m-1}(\hat{\alpha}_x) + J_{n-2m+1}(\hat{\alpha}_x)], \quad (32a)$$

$$\begin{aligned} \hat{I}_z = & 2e^{i\psi_0} \sum_{m,n=-\infty}^{\infty} \left(\frac{\sin \bar{k}\eta}{\bar{k}} \right) J_m(\hat{\alpha}_z) \\ & \cdot \{ \beta_1 J_{n-2m}(\hat{\alpha}_z) + k_0 z_1 [J_{n-2m-2}(\hat{\alpha}_x) + J_{n-2m+2}(\hat{\alpha}_x)] \}, \end{aligned} \quad (32b)$$

and $\hat{I}_y = 0$, where

$$\frac{d^2 I_\theta}{d\omega d\Omega} = \frac{e^2 \omega^2}{4\pi^2 c^3} \left| \hat{I}_x \cos \theta \cos \phi - \hat{I}_z \sin \theta \right|^2, \quad (33a)$$

$$\frac{d^2 I_\phi}{d\omega d\Omega} = \frac{e^2 \omega^2}{4\pi^2 c^3} \left| \hat{I}_x \sin \phi \right|^2. \quad (33b)$$

The frequency width of the radiation spectrum for a given harmonic is determined by the resonance function $R(k, nk_0)$, where

$$R(k, nk_0) = \left(\frac{\sin \bar{k}\eta_0}{\bar{k}\eta_0} \right)^2. \quad (34)$$

This function is sharply peaked about the resonant frequency, ω_n , given by $\bar{k} = 0$,

$$\omega_n = \frac{n\omega_0}{1 - \beta_1(1 + \cos \theta)}. \quad (35)$$

The width of the spectrum, $\Delta\omega$, about ω_n is given by $\Delta\omega/\omega_n = 1/nN_0$, where $N_0 = L_0/\lambda_0$ is the number of periods of the laser field with which the electron interacts.

Since the frequency spectra for two different harmonics, n and n' , are sufficiently well separated, the summations in Eqs. (32a) and (32b) may be simplified to yield

$$\begin{aligned} \frac{d^2 I}{d\omega d\Omega} = \sum_{n=1}^{\infty} \frac{e^2 k^2}{4\pi^2 c} \left(\frac{\sin \bar{k}\eta_0}{\bar{k}} \right)^2 \\ \cdot [C_x^2(1 - \sin^2 \theta \cos^2 \phi) + C_z^2 \sin^2 \theta - C_x C_z \sin 2\theta \cos \phi], \end{aligned} \quad (36)$$

where

$$C_x = \sum_{m=-\infty}^{\infty} (-1)^m k_0 r_1 J_m(\alpha_z) [J_{n-2m-1}(\alpha_x) + J_{n-2m+1}(\alpha_x)], \quad (37a)$$

$$\begin{aligned} C_z = \sum_{m=-\infty}^{\infty} (-1)^m 2J_m(\alpha_z) \{ \beta_1 J_{n-2m}(\alpha_x) \\ + k_0 z_1 [J_{n-2m-2}(\alpha_x) + J_{n-2m+2}(\alpha_x)] \}, \end{aligned} \quad (37b)$$

and

$$\alpha_z = \frac{na_0^2(1 + \cos \theta)}{8h_0^2 [1 - \beta_1(1 + \cos \theta)]}, \quad (38a)$$

$$\alpha_x = \frac{na_0 \sin \theta \cos \phi}{h_0 [1 - \beta_1(1 + \cos \theta)]}. \quad (38b)$$

In the deriving the above expressions, the approximation $\omega \simeq \omega_n$ was made in the arguments of the Bessel functions, α_x and α_z .

Plots of the normalized amplitude of the scattered intensity, $d^2I/d\omega d\Omega$, versus normalized frequency, $\omega/4\gamma_0^2\omega_0$, and normalized observation angle, $\gamma_0\theta$, are shown in Figs. 2(a,b) for the case of a linearly polarized laser ($N_0 = 7$) interacting with a counterpropagating relativistic electron ($\gamma_0 = 5$). The intensity is shown in the plane of electron motion, $\phi = 0$, i.e., θ is the "horizontal" observation angle ($\theta = 0$ is along the z -axis, the axis of propagation). Figure 2(a) shows the intensity in the first two harmonics for $a_0 = 0.5$. Significant radiation occurs only at the fundamental ($n = 1$). The intensity of the fundamental peaks on axis with a frequency shifted slightly from the low-intensity, Thomson backscattered value of $4\gamma_0^2\omega_0$, and is confined to an angle $\theta < 1/\gamma_0$. Figure 2(b) shows the intensity in the first three harmonics for $a_0 = 1.0$. Significant radiation now occurs in the harmonics as well as the fundamental. Only the odd harmonics are finite along the axis ($\theta = 0$) and the frequency shift due to finite a_0 is more apparent. The angular distribution of the higher harmonics is more extensive than the fundamental. The n^{th} harmonic exhibits $(n + 1)/2$, for n odd, or $n/2$, for n even, intensity maxima as a function of θ . For larger values of a_0 , the harmonics dominate the spectrum.

Plots of the normalized amplitude of the scattered intensity, $d^2I/d\omega d\Omega$, versus observation angle, θ , are shown in Figs. 3(a-c) for the case of a linearly polarized laser ($N_0 = 7$) interacting with a dense plasma electron. The intensity is shown in the plane of electron motion, $\phi = 0$, i.e., θ is the horizontal observation angle. Figure 3(a) shows the intensity in first three harmonics for $a_0 = 0.5$, Fig. 3(b) shows the intensity in first six harmonics for $a_0 = 1.0$, and Fig. 3(c) shows the intensity in first twelve harmonics for $a_0 = 2.0$. For a dense plasma, there is no average axial drift of the electrons, hence, harmonic radiation is scattered over large angles and the frequency is not shifted, i.e., $\omega_n = n\omega_0$. (For convenience, the intensity is plotted only at the resonant frequencies, $\omega = \omega_n$.) Only the odd harmonics are finite along the axis ($\theta = 0$) and the intensity is maximum off-axis for all harmonics with $n > 1$. The n^{th} harmonic exhibits $(n + 1)/2$, for n odd, or $n/2$, for n even, intensity maxima as a function of θ within the region $0 \leq \theta \leq \pi/2$.

Backscattered Radiation. Of particular interest is the radiation backscattered along

the axis. In the backscattered direction, $\theta = 0$, only the odd harmonics are finite, i.e., the even harmonics vanish. Setting $\theta = 0$ in the above expressions gives, for the n^{th} odd harmonic,

$$\left. \frac{d^2 I_n}{d\omega d\Omega} \right|_{\theta=0} = e^2 k_0 N_0 M_0^2 F_n(a_0) G_n(\omega), \quad (39)$$

where

$$F_n(a_0) = n\alpha_n [J_{(n-1)/2}(\alpha_n) - J_{(n+1)/2}(\alpha_n)]^2, \quad (40)$$

is the harmonic amplitude function, $\alpha_n = na_0^2/4(1 + a_0^2/2)$,

$$G_n(\omega) = \frac{R(k, nk_0)}{\Delta\omega} = \frac{1}{\Delta\omega} \left[\frac{\sin(\omega - nM_0\omega_0)\bar{T}}{(\omega - nM_0\omega_0)\bar{T}} \right]^2, \quad (41)$$

is the frequency spectrum function and $\bar{T} = L_0/2cM_0$. The function $G_n(\omega)$ is a resonance function sharply peaked about the resonant frequency, $\omega_n = nM_0\omega_0$, with a width given by $\Delta\omega/\omega_n = 1/nN_0$, where the frequency multiplication factor M_0 is given by Eq. (17). Furthermore, $G_n \rightarrow \delta(\omega - \omega_n)$ as $N_0 \rightarrow \infty$.

The energy radiated in the n^{th} backscattered harmonic depends on the function $F_n(a_0)$, Eq. (40). For high harmonics, $n \gg 1$, F_n becomes significant when $a_0^2 \gg 1$. For modest power lasers for which $a_0^2 \ll 1$, only the fundamental, $n = 1$, is significant. A plot of the function F_n versus the parameter $(a_0^2/4)/(1 + a_0^2/2)$ is shown in Fig. 4.

B. Circular Polarization

To calculate the scattered radiation from a circularly polarized incident laser field ($\delta_p = 0$), the orbits given by Eqs. (18)-(19) are used in Eqs. (25a)-(25b). The intensity distribution can be written as

$$\frac{d^2 I_\theta}{d\omega d\Omega} = \frac{e^2 \omega^2}{4\pi^2 c^3} \left| \int_{-\eta_0}^{\eta_0} d\eta \left[\frac{k_0 r_1}{\sqrt{2}} \cos \theta \cos(k_0 \eta - \phi) - \beta_1 \sin \theta \right] \exp(i\psi) \right|^2, \quad (42a)$$

$$\frac{d^2 I_\phi}{d\omega d\Omega} = \frac{e^2 \omega^2}{4\pi^2 c^3} \left| \int_{-\eta_0}^{\eta_0} d\eta \left[\frac{k_0 r_1}{\sqrt{2}} \sin(k_0 \eta - \phi) \right] \exp(i\psi) \right|^2. \quad (42b)$$

The phase, ψ , is given by

$$\psi = \psi_0 + [1 - \beta_1(1 + \cos \theta)] k\eta - (kr_1/\sqrt{2}) \sin \theta \sin(k_0 \eta - \phi), \quad (43)$$

where ψ_0 is given by Eq. (27b). Using the Bessel identity, Eq. (28), gives

$$\exp\{i[\psi + \ell(k_0\eta - \phi)]\} = \sum_{n=-\infty}^{\infty} \exp[i(\psi_0 + \bar{k}\eta + n\phi)] J_{n+\ell}(\hat{\alpha}), \quad (44)$$

where $\hat{\alpha} = (kr_1/\sqrt{2}) \sin \theta$ and where \bar{k} is given by Eq. (30a). This allows the calculation of the integrals in Eqs. (42a) and (42b). In particular,

$$\begin{aligned} \hat{I}_0 &= \int_{-\eta_0}^{\eta_0} d\eta \exp(i\psi) \\ &= \sum_{n=-\infty}^{\infty} \exp[i(\psi_0 + n\phi)] \left(\frac{\sin \bar{k}\eta_0}{\bar{k}} \right) 2J_n(\hat{\alpha}), \end{aligned} \quad (45a)$$

$$\begin{aligned} \hat{I}_1 &= \int_{-\eta_0}^{\eta_0} d\eta \cos(k_0\eta - \psi) \exp(i\psi) \\ &= \sum_{n=-\infty}^{\infty} \exp[i(\psi_0 + n\phi)] \left(\frac{\sin \bar{k}\eta_0}{\bar{k}} \right) \frac{2n}{\hat{\alpha}} J_n(\hat{\alpha}), \end{aligned} \quad (45b)$$

$$\begin{aligned} \hat{I}_2 &= \int_{-\eta_0}^{\eta_0} d\eta \sin(k_0\eta - \psi) \exp(i\psi) \\ &= \sum_{n=-\infty}^{\infty} \exp[i(\psi_0 + n\phi)] \left(\frac{\sin \bar{k}\eta_0}{\bar{k}} \right) 2iJ'_n(\hat{\alpha}). \end{aligned} \quad (45c)$$

As indicated by Eq. (34), the above expressions imply a frequency spectrum centered about $\omega = \omega_n$, where ω_n is given by Eq. (35), of width $\Delta\omega/\omega_n = 1/nN_0$. Since the frequency spectra of two different harmonics, n and n' , are well separated, the summations in Eqs. (42a)-(42b) can be simplified. Using Eqs. (42) and (45), the radiation spectrum can be written as

$$\begin{aligned} \frac{d^2 I}{d\omega d\Omega} &= \sum_{n=1}^{\infty} \frac{e^2 k^2}{\pi^2 c} \left(\frac{\sin \bar{k}\eta_0}{\bar{k}} \right)^2 \\ &\quad \cdot \left\{ \frac{[\cos \theta - \beta_1(1 + \cos \theta)]^2}{\sin^2 \theta} J_n^2(\alpha) + \frac{k_0^2 r_1^2}{2} J_n'^2(\alpha) \right\}, \end{aligned} \quad (46)$$

where $k_0 r_1 = a_0/h_0$ and the approximation $\omega \simeq \omega_n$ has been made in the arguments of the Bessel functions, i.e.,

$$\alpha = \frac{n(a_0/\sqrt{2}) \sin \theta}{h_0 [1 - \beta_1(1 + \cos \theta)]}. \quad (47)$$

In the above expression, the terms proportional to $J_n(\alpha)$ are the contributions from I_θ , and the terms proportional to $J'_n(\alpha)$ are the contributions from I_ϕ .

Using the identities [1]

$$\begin{aligned}\sum_{n=1}^{\infty} n^2 J_n^2(n\hat{z}) &= \frac{\hat{z}^2(4 + \hat{z}^2)}{16(1 - \hat{z}^2)^{7/2}}, \\ \sum_{n=1}^{\infty} n^2 J_n'^2(n\hat{z}) &= \frac{(4 + 3\hat{z}^2)}{16(1 - \hat{z}^2)^{5/2}},\end{aligned}\tag{48}$$

the summation in Eq. (46) can be carried out and an expression for $dI/d\Omega$ can be found. After integrating over frequency, one finds

$$\begin{aligned}\frac{dI}{d\Omega} &= \frac{(e^2/c)N_0\omega_0 a_0^2/h_0^2}{32(1 - \hat{z}^2)^{7/2} [1 - \beta_1(1 + \cos\theta)]^3} \\ &\cdot \left\{ \frac{[\cos\theta - \beta_1(1 + \cos\theta)]^2}{[1 - \beta_1(1 + \cos\theta)]^2} (4 + \hat{z}^2) + (4 + 3\hat{z}^2)(1 - \hat{z}^2) \right\},\end{aligned}\tag{49}$$

where $\hat{z} = \alpha/n$.

Plots of the normalized amplitude of the scattered intensity, $d^2I/d\omega d\Omega$, versus normalized frequency, $\omega/4\gamma_0^2\omega_0$, and normalized observation angle, $\gamma_0\theta$, are shown in Figs. 5 and 6 for the case of a circularly polarized laser ($a_0 = 1$, $N_0 = 7$). Because of the symmetry of the electron orbit, the intensity distribution is independent of ϕ . Figure 5 shows the scattered intensity from a counterpropagating relativistic electron ($\gamma_0 = 5$) for the first three harmonics. Only the fundamental ($n = 1$) is nonzero on axis, where its intensity is maximum, and its frequency is shifted from the low-intensity, Thomson backscattered value of $4\gamma_0^2\omega_0$. The intensity of the higher harmonics peak off-axis and is confined to angles $\theta \lesssim 2/M_0^{1/2}$, as discussed in Sect. IV C below. Figure 6 shows the scattered intensity from an electron in a dense plasma for the first six harmonics. For a dense plasma, there is no average axial drift of the electrons and the frequency is not shifted, i.e., $\omega_n = n\omega_0$. Only the fundamental is nonzero on axis, where its intensity is maximum. For higher harmonics, the intensity is maximum in the transverse direction, $\theta = \pi/2$. As the intensity of the laser pulse increases, more radiation is scattered into the higher harmonics.

Backscattered Radiation. In the backscattered direction, only the fundamental, $n = 1$,

is nonzero. In the limit $\theta \rightarrow 0$, $J_1'(\alpha) \rightarrow 1/2$ and $J_1(\alpha) \rightarrow \alpha/2$. Hence,

$$\frac{d^2 I_n}{d\omega d\Omega} \Big|_{\theta=0} = \frac{e^2 k_0 N_0 M_0^2 a_0^2}{4(1 + a_0^2/2)} G_1(\omega), \quad (50)$$

where $G_1(\omega)$ is given by Eq. (41) with $n = 1$.

IV. RADIATION PROPERTIES

A. Radiated Power

The power radiated by a single electron, P_s , undergoing relativistic quiver motion in an intense laser field can be calculated from the relativistic Larmor formula [24]

$$P_s = \frac{2e^2}{3c} \gamma^2 \left[\left(\frac{d\mathbf{u}}{dt} \right)^2 - \left(\frac{d\gamma}{dt} \right)^2 \right]. \quad (51)$$

Assuming the electron orbit is a function of only the variable $\eta = z + ct$,

$$P_s = \frac{2}{3} e^2 c (\gamma + u_z)^2 \left[\left(\frac{d\mathbf{u}}{d\eta} \right)^2 - \left(\frac{d\gamma}{d\eta} \right)^2 \right]. \quad (52)$$

Using the orbits described in Sec. II, the power radiated by an electron in the presence of a circularly or linearly polarized radiation field is given by

$$P_s \simeq \frac{2}{3} e^2 c h_0^2 k_0^2 a_0^2 \cdot \begin{cases} 1/2, & \text{circular,} \\ \sin^2 k_0 \eta, & \text{linear,} \end{cases} \quad (53)$$

where h_0 is given by Eq. (12). Averaging the above expression over a laser period, the ratio of the radiated power to the incident laser power, P_s/P_0 , can be written as

$$P_s/P_0 \simeq 16r_e^2 h_0^2 / 3r_0^2, \quad (54)$$

where $r_e = e^2/m_e c^2$ is the classical electron radius.

The total power radiated by a laser pulse passing through a uniform distribution of electrons with a constant density n_0 is given by $P_T = N_e P_s$, where $N_e = n_0 L_0 \sigma_L$ is the total number of electrons interacting with the laser pulse at a given time, $L_0 = c\tau_L$ is the laser pulse length and σ_L is the effective cross-section. Assuming a Gaussian laser pulse, $\hat{a} = (a_0 r_0 / r_L) \exp(-r^2 / r_L^2)$, where r_L is the laser spot size and r_0 is the minimum spot size, the effective cross-section, σ_L , can be found by letting $a_0 \rightarrow \hat{a}$ in Eq. (54) and integrating P_s over r . One finds

$$\sigma_L = \frac{\pi r_0^2}{2} \cdot \begin{cases} 1, & \text{e-beam,} \\ f_p, & \text{plasma,} \end{cases} \quad (55)$$

where $f_p = (1 + a_0^2/4)/(1 + a_0^2/2)$. In Eq. (55), the top expression holds in the short pulse (electron beam) limit, i.e., $h_0 = \gamma_0(1 + \beta_0)$, and the bottom expression holds in the long pulse (plasma) limit, i.e., $h_0 = (1 + a_0^2/2)^{1/2}$. Hence, the total scattered power by a uniform electron density n_0 is given by

$$P_T/P_0 = (8\pi/3)r_e^2 L_0 n_0 f_p h_0^2. \quad (56)$$

As example, a $n_0 = 10^{20} \text{ cm}^{-3}$ plasma interacting with a 1 ps laser pulse with $a_0 = 5$ gives $P_T/P_0 = 1.4 \times 10^{-5}$. The ratio of the total scattered energy to the laser pulse energy is approximately $P_T L/P_0 L_0$, where L is the total length over which the laser pulse interacts with the electrons.

B. Resonance Function

Several properties of the radiation spectra can be ascertained by examining the resonance function, $R(k, nk_0)$, given by Eq. (34). The function $R(k, nk_0)$ is sharply peaked about the resonant harmonic frequencies, ω_n , defined by $\bar{k} = 0$, which can be written as

$$\omega_n = \frac{nM_0\omega_0}{[1 + M_0\beta_1(1 - \cos\theta)]}, \quad (57)$$

where n is the harmonic number and M_0 is the relativistic doppler upshift factor. For a plasma, $\beta_1 = 0$ and $M_0 = 1$, which gives $\omega_n = n\omega_0$, independent of θ . For a relativistic electron beam with $M_0 \gg 1$, the radiation is primarily backscattered into small angles, $\theta^2 \ll 1$. Hence $\omega_n \simeq nM_0\omega_0/(1 + M_0\theta^2/4)$, which indicates a maximum frequency in the backscattered direction along the axis, $\theta = 0$. The change in frequency $\Delta\omega$ with respect to a change in angle $\Delta\theta$ is given by

$$\frac{|\Delta\omega|}{\omega_n} \simeq \frac{|M_0(\theta\Delta\theta + \Delta\theta^2/2)|}{(2 + M_0\theta^2/2)}, \quad (58)$$

assuming $M_0 \gg 1$. Alternatively, Eq. (58) can be solved to give the angular spread $\Delta\theta$ about θ over which a given bandwidth $\Delta\omega$ about ω_n may occupy. For a relativistic electron beam with $M_0 \gg 1$, two angles are of particular interest. It is shown below that for a linearly polarized laser, the radiation intensity for the higher harmonics, $n \gg 1$, is centered

about $\theta = 0$, whereas for circular polarization, the intensity is centered about $\theta_0 = 2/M_0^{1/2}$. For these two angles, Eq. (58) implies

$$\Delta\theta \simeq \frac{\gamma_{\perp}}{\gamma_0} \cdot \begin{cases} (\Delta\omega/\omega_n)^{1/2}, & \text{for } \theta = 0, \\ (\Delta\omega/\omega_n), & \text{for } \theta = \theta_0, \end{cases} \quad (59)$$

where $M_0 \simeq 4\gamma_0^2/\gamma_{\perp}^2$ has been used.

The intrinsic (i.e., associated with the radiation from a single electron) frequency width $\Delta\omega_n$ of the radiation about a resonant frequency ω_n can be found by letting $\omega = \omega_n + \delta\omega$ and integrating the function $R(k, nk_0)$ over $\delta\omega$, which gives

$$\Delta\omega_n = \int_{-\infty}^{\infty} d(\delta\omega) R(k, k_0) = \omega_n/nN_0. \quad (60)$$

Hence, $\Delta\omega_n/\omega_n = 1/nN_0$, where $N_0 = L_0/\lambda_0$ is the number of wavelengths in the laser pulse. Furthermore, $R(k, nk_0) \rightarrow \Delta\omega_n \delta(\omega - \omega_n)$ as $N_0 \rightarrow \infty$. The angular width $\Delta\theta_n$ within which can be found radiation with frequencies in $\Delta\omega_n$ about ω_n , for a single harmonic n , is given by inserting Eq. (60) in Eq. (59),

$$\Delta\theta_n \simeq \frac{\gamma_{\perp}}{\gamma_0} \cdot \begin{cases} (1/nN_0)^{1/2}, & \text{for } \theta = 0, \\ (1/nN_0), & \text{for } \theta = \theta_0. \end{cases} \quad (61)$$

Alternatively, similar expressions can be obtained by letting $\theta = \theta' + \delta\theta$ and integrating $R[k_n(\theta'), k_0]$ over $\delta\theta$. It should be pointed out that Eqs. (59) and (61) apply to relativistic electron beams with $M_0 \gg 1$. For plasmas, the angular width occupied by a given $\Delta\omega$ about ω_n must be determined by considering the full functional form of the radiation spectrum, Eqs. (36) and (46), not just the resonance function $R(k, nk_0)$.

C. Ultra-Intense Behavior

For values of $a_0 \ll 1$, the scattered radiation will be narrowly peaked about the fundamental resonant frequency, $\omega_1 = \omega_0/[1 - \beta_1(1 + \cos\theta)]$. As a_0 approaches unity, scattered radiation will appear at harmonics of the resonant frequency as well, $\omega_n = n\omega_1$. When $a_0 \gg 1$, high harmonic ($n \gg 1$) radiation is generated and the resulting synchrotron radiation spectrum consists of many closely spaced harmonics. Finite electron energy

spread effects can broaden the linewidth causing the radiation from the various harmonics to overlap. For example, a finite thermal axial velocity spread will lead to overlap when $(\Delta\omega/\omega_n)_{th} \gtrsim 1/n$, where $(\Delta\omega/\omega_n)_{th}$ is given below by Eq. (77). Hence, in the ultra-intense limit, i.e., $a_0 \gg 1$, the gross spectrum appears broadband, and a continuum of radiation is generated which extends out to a critical frequency, ω_c , beyond which the radiation intensity diminishes. The critical frequency can be written as $\omega_c = n_c \omega_R$, where n_c is the critical harmonic number. It is possible to calculate n_c by examining the radiation spectrum, Eqs. (36) and (46), in the ultra-intense limit, $a_0 \gg 1$.

Asymptotic properties of the radiation spectrum for large harmonic numbers, $n \gg 1$, can be analyzed using the relationships [25]

$$\begin{aligned} J_n(n\hat{z}) &\simeq \frac{\hat{x}^{1/2}}{\pi} (1 - \hat{z}^2)^{-1/4} K_{1/3}(n\hat{x}), \\ J'_n(n\hat{z}) &\simeq -\frac{\hat{x}^{1/2}}{\pi\hat{z}} (1 - \hat{z}^2)^{1/4} K_{2/3}(n\hat{x}), \end{aligned} \quad (62)$$

where $|\hat{z}| < 1$ and is a function of a_0 and θ ,

$$\hat{x} = \ln \left[1 + (1 - \hat{z}^2)^{1/2} \right] - \ln \hat{z} - (1 - \hat{z}^2)^{1/2}, \quad (63)$$

and $K_{1/3}$, $K_{2/3}$ are modified Bessel functions. In particular, for $n\hat{x} \gg 1$,

$$K_{1/3} \simeq K_{2/3} \simeq (\pi/2n\hat{x}) \exp(-n\hat{x}), \quad (64)$$

and, hence, only harmonic radiation with $n\hat{x} \lesssim 1$ will contribute significantly to the spectrum. The critical harmonic number is defined as $n_c \hat{x}_{min} = 1$, i.e., $n_c = 1/\hat{x}_{min}$, where \hat{x}_{min} is the minimum value of Eq. (63). Furthermore, $d\hat{x}/d\hat{z} < 0$ and the minimum of \hat{x} occurs at \hat{z}_{max} . Typically, for $a_0^2 \gg 1$, $1 - \hat{z}_{max}^2 \ll 1$ and Eq. (63) can be expanded to yield, to leading order, $\hat{x}_{min} \simeq (1/3) (1 - \hat{z}_{max}^2)^{3/2}$. The critical harmonic number is given by the inverse of this expression.

1. Circular Polarization

For a circularly polarized incident laser field, $\hat{z} = \alpha/n$, where α is given by Eq. (47), i.e.,

$$\hat{z} = \frac{(a_0/\sqrt{2}) \sin \theta}{h_0 [1 - \beta_1(1 + \cos \theta)]}. \quad (65)$$

For a fixed value of $a_0 \gg 1$, the maximum value of \hat{z} is given by $\hat{z}_{max} = (a_0/\sqrt{2})/(1 + a_0^2/2)^{1/2}$, and occurs at an angle θ_0 given by

$$\cos \theta_0 = (M_0 - 1)/(M_0 + 1). \quad (66)$$

Inserting this value of \hat{z}_{max} into Eq. (63) gives, for $a_0^2 \gg 1$, $\hat{x}_{min} \simeq 2\sqrt{2}/3a_0^3$ and, hence,

$$n_c \simeq 3a_0^3/2\sqrt{2}. \quad (67)$$

Furthermore, radiation at the harmonic n_c will be scattered in the direction $\theta = \theta_0$, where θ_0 is given by Eq. (66). The frequency of the radiation scattered in the direction $\theta = \theta_0$ is given by

$$\omega(\theta = \theta_0) = n\omega_0(M_0 + 1)/2. \quad (68)$$

For a plasma, $M_0 = 1$ and $\theta_0 = \pm\pi/2$, i.e., the high harmonic radiation will be scattered perpendicular to the incident laser field. For a relativistic electron beam with $M_0 \gg 1$, $\theta_0 \simeq 2/M_0^{1/2}$ and the high harmonic radiation is nearly backscattered. Physically, θ_0 is related to the pitch angle of the electron orbit, $|u_\perp|/|u_z| \simeq 2\sqrt{2}/M_0^{1/2} \simeq a_0/\gamma_0$, assuming $a_0^2 \gg 1$ and $M_0 \gg 1$.

The asymptotic properties ($n \gg 1$) of the radiation spectra can be readily obtained from Eqs. (46) and (62). In the ultra-relativistic limit, $a_0^2 \gg 1$, the radiation is confined to small angles $\delta\theta$ about the optimum angle θ_0 . i.e., $\theta = \theta_0 + \delta\theta$, where $\delta\theta^2 \ll 1$. Assuming $n \gg 1$, $a_0^2 \gg 1$ and $\delta\theta^2 \ll 1$, Eqs. (46) and (62) give

$$\frac{d^2I}{d\omega d\Omega} \simeq N_0 \frac{3e^2}{\pi^2 c} \frac{\gamma^2 \xi^2}{(1 + \gamma^2 \delta\theta^2)} \left[\frac{\gamma^2 \delta\theta^2}{(1 + \gamma^2 \delta\theta^2)} K_{1/3}^2(\xi) + K_{2/3}^2(\xi) \right], \quad (69)$$

where

$$\xi = \frac{\omega}{\omega_c} (1 + \gamma^2 \delta\theta^2)^{3/2}, \quad (70a)$$

$$\omega_c = n_c \frac{(M_0 + 1)}{2} \omega_0, \quad (70b)$$

$$\gamma = \frac{a_0(M_0 + 1)}{2(2M_0)^{1/2}}. \quad (70c)$$

Equation (69) holds for arbitrary values of M_0 , i.e., electron beams of arbitrary energies as well as stationary plasmas. In Eq. (70a), $n_c = 3a_0^3/2\sqrt{2}$ and the factor $(M_0 + 1)/2$ is the

relativistic doppler upshift for radiation scattered at the optimum angle θ_0 , as indicated by Eq. (68). The expression for γ follows from Eq. (8b) assuming $a_0^2 \gg 1$. In deriving Eq. (69), Eq. (62) was used and the summation was approximated by an integral, i.e., $\sum_n R(k, nk_0) \simeq 1/N_0$ and, hence, $n\hat{x} \rightarrow \xi$.

Notice in the limit $\delta\theta = 0$, $d^2I/d\omega d\Omega \sim \xi^2 K_{2/3}^2(\xi)$, where $\xi = \omega/\omega_c$. A plot of the function $Y(\xi) = \xi^2 K_{2/3}^2(\xi)$ is shown in Fig. 7. The function $Y(\xi)$ is maximum at $\xi = 1/2$ and decreases rapidly for $\xi > 1$. Half the total power is radiated at frequencies $\omega < \omega_c/2$ and half at $\omega > \omega_c/2$. This can be shown by integrating $d^2I/d\omega d\Omega$ over frequency and angle [10], i.e., integrating the expression given below by Eq. (71b) over frequency.

Equation (69) is N_0 times the standard result [24] for the synchrotron radiation spectrum emitted from an electron moving in an instantaneously circular orbit in the ultra-relativistic limit with a radius of curvature $\rho = 3\gamma^3 c/\omega_c$. Several well-known properties [24] follow from Eq. (69), for example

$$\frac{dI}{d\Omega} \simeq \frac{7e^2}{48c} \frac{N_0 \omega_c \gamma^2}{(1 + \gamma^2 \delta\theta^2)^{5/2}} \left[1 + \frac{5}{7} \frac{\gamma^2 \delta\theta^2}{(1 + \gamma^2 \delta\theta^2)} \right], \quad (71a)$$

$$\frac{dI}{d\omega} \simeq 2\sqrt{3} \frac{e^2}{c} N_0 \gamma \frac{\omega}{\omega_c} \int_{2\omega/\omega_c}^{\infty} d\xi K_{5/3}(\xi). \quad (71b)$$

The peak intensity is of the order $N_0 e^2 \gamma/c$ and the total radiated energy is of the order $N_0 e^2 \gamma \omega_c/c$. The peak intensity occurs at the optimum angle θ_0 , i.e., $\delta\theta = 0$, at approximately the critical frequency, $\omega \simeq \omega_c$, i.e., $n \simeq n_c = 3a_0^3/2\sqrt{2}$. For harmonics below n_c , ($\omega \ll \omega_c$), the radiation intensity increases as $(\omega/\omega_0)^{2/3}$, and above n_c ($\omega \gg \omega_c$), the radiation intensity decreases exponentially, i.e.,

$$\left. \frac{d^2I}{d\omega d\Omega} \right|_{\delta\theta=0} \simeq N_0 \frac{3e^2}{\pi^2 c} [\Gamma(2/3)]^2 \gamma^2 \left(\frac{\omega}{2\omega_c} \right)^{2/3}, \quad \omega \ll \omega_c, \quad (72a)$$

$$\left. \frac{d^2I}{d\omega d\Omega} \right|_{\delta\theta=0} \simeq N_0 \frac{3e^2}{2\pi c} \gamma^2 \left(\frac{\omega}{\omega_c} \right) \exp\left(-\frac{2\omega}{\omega_c}\right), \quad \omega \gg \omega_c. \quad (72b)$$

Furthermore, for $\omega \ll \omega_c$, the scattered radiation at a fixed frequency is confined to an angular spread $\Delta\delta\theta = (\omega_c/\omega)^{1/3}/\gamma$ about θ_0 , whereas for $\omega > \omega_c$, $\Delta\delta\theta = (\omega_c/3\omega)^{1/2}/\gamma$. The average angular spread for the frequency integrated spectrum is $\langle \delta\theta^2 \rangle^{1/2} \sim 1/\gamma$.

As an example, the peak intensity in the transverse direction ($\theta = \pi/2$) of each harmonic, $\omega = n\omega_0$, is shown in Fig. 8 for the case of a high intensity, circularly polarized

laser pulse encountering an electron in a dense plasma. Plots for two different intensities are shown, $a_0 = 4$ and $a_0 = 6$. The arrows indicate the approximate critical harmonic number, $n_c \simeq a_0^3$, for each case. Asymptotically, $a_0 \gg 1$, this curve approaches the form $Y(\xi) = \xi^2 K_{2/3}^2(\xi)$, shown in Fig. 7.

2. Linear Polarization

For a linearly polarized incident laser field in the limit $a_0 \ll 1$, upshifted radiation at the fundamental frequency is generated in a narrow cone about the backscattered direction, $\Omega \simeq 2\pi\theta_c^2$, where $\theta_c \sim 1/h_0$. However, in the limit $a_0 \gg 1$, a near-continuum of high harmonic radiation is generated and the emission cone about backscattered direction widens [10]. In particular, in the vertical direction, $\phi = \pi/2$ (the direction normal to the x - z plane which contains the electron orbit), emission is confined to the vertical angle $\theta_v \sim 1/h_0$. In the horizontal direction, $\phi = 0$ (in the plane of the electron orbit), the emission angle widens and is confined the horizontal angle $\theta_h \sim a_0/h_0$, which is determined by the deflection angle of the electron in the x - z plane [10]. The asymptotic properties of the radiation spectrum can be analyzed using Eqs. (36) and (62). Letting θ represent the observation angle in the vertical direction, i.e., $\phi = \pi/2$, then in the limits $a_0 \gg 1$ and $n \gg 1$, $\theta^2 \ll 1$ and the coefficients C_x and C_z occurring in Eq. (36) are given by $C_x^2 \simeq J_\ell^2(\ell\hat{z})$ and $C_z^2 \simeq (a_0/h_0)^2 J_\ell'^2(\ell\hat{z})$, where additional terms of order $1/a_0$ have been neglected and $n = 2\ell + 1 \gg 1$. Here, for linear polarization,

$$\hat{z} = \frac{\alpha_z}{\ell} \simeq 1 - \frac{2}{a_0^2} \left(1 + \frac{h_0^2}{4} \theta^2 \right). \quad (73)$$

The asymptotic spectrum near the axis can be found by using the asymptotic properties of the Bessel functions, Eq. (62). Notice that for $\theta = 0$, $\hat{x}_{max} \simeq 8/3a_0^3$. Hence, $\ell_c = 1/\hat{x}_{max}$, and the critical harmonic number, $n_c \simeq 2\ell_c$ is given by

$$n_c \simeq 3a_0^3/4. \quad (74)$$

Using Eqs. (36) and (62), the asymptotic spectrum is given by

$$\frac{d^2I}{d\omega d\Omega} \simeq N_0 \frac{12e^2}{\pi^2 c} \frac{\hat{\gamma}^2 \zeta^2}{(1 + \hat{\gamma}^2 \theta^2)} \left[\frac{\hat{\gamma}^2 \theta^2}{(1 + \hat{\gamma}^2 \theta^2)} K_{1/3}^2(\zeta) + K_{2/3}^2(\zeta) \right], \quad (75)$$

where

$$\zeta = \frac{\omega}{\omega_c} (1 + \hat{\gamma}^2 \theta^2)^{3/2}, \quad (76a)$$

$$\omega_c = n_c M_0 \omega_0, \quad (76b)$$

$$\hat{\gamma} = h_0/2. \quad (76c)$$

In deriving Eq. (75), $\sum_n R(k, nk_0) \rightarrow 1/N_0$ and $l\hat{x} \rightarrow \zeta$. Several subsequent properties of the asymptotic spectrum follow from Eq. (75). As was the case for circular polarization, Eqs. (71)-(72) apply, with $N_0 \rightarrow 4N_0$, $\delta\theta \rightarrow \theta$, $\gamma \rightarrow \hat{\gamma}$ and where ω_c is given by Eq. (76b). In particular, radiation with $\omega \simeq \omega_c$ is confined to a vertical angle $\theta_v \simeq 1/\hat{\gamma}$. In the horizontal direction, emission is confined to the angle $\theta_h \sim a_0/\hat{\gamma}$, i.e., $\theta_h \sim a_0/\gamma_0$ for an electron beam and $\theta_h \sim \pi/2$ for a plasma.

As an example, the peak intensity on axis ($\theta = 0$) of the odd harmonics, $\omega = nM_0\omega_0$, is shown in Fig. 9 for the case of a high intensity, linearly polarized laser pulse encountering a counterstreaming relativistic electron ($\gamma_0 = 5$). Plots for two different intensities are shown, $a_0 = 4$ and $a_0 = 6$. The arrows indicate the approximate critical harmonic number, $n_c \simeq 3a_0^3/4$, for each case. Note that the harmonic intensity is plotted versus the normalized frequency $\omega/4\gamma_0^2\omega_0 \simeq 1.5a_0$. Asymptotically, $a_0 \gg 1$, this curve approaches the form $Y(\xi) = \xi^2 K_{2/3}^2(\xi)$, shown in Fig. 7.

V. NON-IDEAL EFFECTS

A. Electron Energy Spread

The above analysis has assumed ideal electron distributions, i.e., thermal and energy spread effects have been neglected. These effects are important in determining the frequency line width of the scattered radiation [10]. For example, the resonance function $R(k, nk_0)$ indicates that if a thermal axial velocity spread Δv_{th} is introduced, i.e., $\beta_z = \beta_0 + \Delta\beta_{th}$, where $\Delta\beta_{th} = \Delta v_{th}/c$, then the scattered radiation along the axis will be shifted in frequency away from ω_n by $\Delta\omega_{th}$, where

$$(\Delta\omega/\omega_n)_{th} = 2\gamma_0^2 \Delta\beta_{th}. \quad (77)$$

For a plasma, $\Delta\beta_{th}$ is related to the initial plasma thermal energy, E_{th} , by $\Delta\beta_{th} = (2E_{th}/m_e c^2)^{1/2}$. For an electron beam, $\Delta\beta_{th}$ is related to the initial normalized energy spread, $\Delta\gamma/\gamma_0$, by $\Delta\beta_{th} = \Delta\gamma/\gamma_0^3 \beta_0$. As an example, a plasma with a temperature of 100 eV would produce a thermal bandwidth of $(\Delta\omega/\omega_n)_{th} \simeq 4\%$.

In actual electron beams, the electrons may have an average angular spread as well as an average energy spread, represented by emittance and intrinsic energy spread, respectively. The normalized beam emittance is given by $\epsilon_n = \gamma_0 r_b \theta_b$, where r_b is the average electron beam radius and θ_b is the average electron angular spread. The fractional longitudinal beam energy spread due to emittance is $(\Delta E/E_b)_\epsilon = \epsilon_n^2/2r_b^2$, where E_b is the initial beam energy. Electron beams may also have an intrinsic energy spread, $(\Delta E/E_b)_i$, due to various reasons, such as, voltage variation, finite pulse length effects, etc. The total spectral width of the radiation about the harmonic ω_n is

$$(\Delta\omega/\omega_n)_T \simeq [(\Delta\omega/\omega_n)_0^2 + (\Delta\omega/\omega_n)_\epsilon^2 + (\Delta\omega/\omega_n)_i^2]^{1/2}, \quad (78)$$

where $(\Delta\omega/\omega_n)_0 = 1/nN_0$ is the finite interaction length spectral width contribution, $(\Delta\omega/\omega_n)_\epsilon = \epsilon_n^2/r_b^2$ is the emittance broadened spectral width and $(\Delta\omega/\omega_n)_i = 2(\Delta E/E_b)_i$ is the intrinsic energy spread broadening contribution. The radiation with total spectral width $(\Delta\omega/\omega_n)_T$ is confined to the angle $\theta_T \simeq (\Delta\omega/\omega_n)_T^{1/2}/\gamma_0$. This consequently reduces the spectral intensity, $d^2I/d\omega d\Omega$, of the scattered radiation from an electron beam for a particular harmonic by approximately θ_0^2/θ_T^2 .

If a particular application requires a bandwidth $(\Delta\omega/\omega_n)_S \leq 1$, this radiation can be found within the angle θ_Σ , where

$$\theta_\Sigma^2 \simeq \theta_S^2 + \theta_T^2 = [(\Delta\omega/\omega_n)_S + (\Delta\omega/\omega_n)_T] / \gamma_0^2. \quad (79)$$

If a bandwidth $(\Delta\omega/\omega_n)_S \gg (\Delta\omega/\omega_n)_T$ is required, all the radiation within a cone of half-angle $\theta_\Sigma \simeq \theta_S = (\Delta\omega/\omega_n)_S^{1/2} / \gamma_0$ can be used. To obtain a bandwidth $(\Delta\omega/\omega_n)_S \ll (\Delta\omega/\omega_n)_T$, the radiation within the cone $\theta_\Sigma \simeq \theta_T = (\Delta\omega/\omega_n)_T^{1/2} / \gamma_0$ must be filtered using a monochromator. As an illustration, for an rf linac electron beam with $\epsilon_n \simeq 5$ mm-mrad, $r_b = 50 \mu\text{m}$ and $\gamma_0 = 100$, $(\Delta E/E_b)_\epsilon \simeq 0.5\%$ and $(\Delta\omega/\omega_n)_\epsilon \simeq 1\%$. Since the intrinsic energy spread is typically $\sim 1\%$ and $N_0 \gtrsim 300$, the total spectral width of the unfiltered LSS radiation is typically $(\Delta\omega/\omega_n)_T \simeq 1\%$ and is confined to the angle $\theta_T \simeq 1$ mrad.

B. Electron Beam Energy Loss

As the electron beam radiates via nonlinear Thomson scattering, the electron beam will lose energy. The rate of loss of electron beam energy is equal to the scattered power, $m_e c^2 d\gamma/dt = -P_s$, where P_s is given by Eq. (54). Assuming $h_0 \simeq 4\gamma^2$, the electron beam energy will evolve [5] according to $\gamma = \gamma_0 / (1 + t/\tau_R)$, where t is the electron beam-laser interaction time and $\tau_R = 3 / (4cr_e k_0^2 a_0^2 \gamma_0)$, where a linearly polarized laser field has been assumed. In practical units, this can be written as

$$\tau_R[\text{ps}] \simeq 1.6 \times 10^{22} E_b^{-1} [\text{MeV}] I_0^{-1} [\text{W}/\text{cm}^2]. \quad (80)$$

One consequence of the loss of electron beam energy is the introduction of an additional source of enhanced bandwidth, $(\Delta\omega/\omega_n)_R = 2(\gamma_0 - \gamma) / \gamma_0$, where $\gamma_0 - \gamma = \gamma t / \tau_R$. For typical values of laser pulse lengths and intensities of interest, $t/\tau_R \ll 1$, and this effect is small. As an example, a 2 ps ($t = 1$ ps) laser pulse with intensity $I_0 = 2.6 \times 10^{17}$ W/cm² ($a_0 = 0.43$) interacting with a $E_b = 40$ MeV ($\gamma_0 = 79$) electron beam gives $(\Delta\omega/\omega_n)_R \simeq 0.13\%$.

C. Ponderomotive Density Depletion

In a high density plasma, the transverse ponderomotive force from the radial gradients in the laser pulse profile can displace the plasma electrons leading to a density depression

on axis. In the long pulse limit, the density depression can be calculated by equating the electrostatic force with the ponderomotive force, $\nabla_{\perp}\phi = \nabla_{\perp}\gamma_{\perp}$, which is the adiabatic response of the plasma electrons to the transverse ponderomotive force [23,26]. This gives an equilibrium density profile of

$$n_e/n_0 = 1 + k_p^{-2}\nabla_{\perp}^2(1 + a^2/2)^{1/2}, \quad (81)$$

where $n_e/n_0 \geq 0$ has been assumed. Assuming a Gaussian transverse profile of the form $|a| \sim \exp(-r^2/\tau_0^2)$, Eq. (81) indicates that the density along the axis is given by

$$\frac{n_e(r=0)}{n_0} = 1 - \frac{a_0^2\lambda_p^2}{2\pi^2\tau_0^2} \left(1 + \frac{a_0^2}{2}\right)^{-1/2}, \quad (82)$$

where $\lambda_p = 2\pi/k_p$. As an example, a high-density plasma with $\tau_0 = 15 \mu\text{m}$, $\lambda_p = 5 \mu\text{m}$ and $a_0 = 7$ gives a density depression along the axis of $\Delta n_e/n_0 = 5\%$. This density depression reduces the total number of electrons scattering radiation, hence, the total scattered power $P_n \sim n_e$ will be reduced. Furthermore, in a high density plasma, the effects of relativistic self-focusing, which occurs for pump laser powers above a critical power, $P_c[\text{GW}] \simeq 17(\lambda_p/\lambda_0)^2$, along with the effects of a density depletion on axis, can provide optical guiding and significantly extend the laser-plasma interaction distance [5,22,23,26,27]. For a relativistic electron beam in the short pulse limit, $\tau_L \ll \gamma_0^3/\omega_p$, the magnitude of the electron density perturbation, Δn_e , due to the ponderomotive force, is given by $|\Delta n_e/n_0| \lesssim (L_0 a_0/\gamma_0 \tau_0)^2 \ll 1$, consistent with the discussion at the end of Section II.

D. Plasma Dispersion

The frequency of the scattered radiation can be affected by the dispersion properties of electromagnetic radiation in a plasma. In the long pulse limit, the nonlinear dispersion relation for radiation of frequency ω and wavenumber k is given [5] by $\omega^2 \simeq c^2 k^2 + \omega_p^2/\gamma_{\perp}$. Notice that the dispersion relation is different for radiation within the region of the pump laser pulse, $\gamma_{\perp} = (1 + a_0^2/2)^{1/2}$, and for radiation propagating in the plasma outside of the pump laser pulse, $\gamma_{\perp} = 1$. In particular, for backscattered radiation, the radiation will transit a counterstreaming boundary region at the trailing edge of the pump laser pulse. As the backscattered radiation transits this boundary region, counterstreaming at the

group velocity of the pump laser pulse, v_g , the frequency and wavenumber of the scattered radiation will be shifted [28]. Hence, the detected frequency, ω_d , of the backscattered radiation will be shifted from the frequency at which it is scattered, ω , within the laser pulse. The detected frequency ω_d is related to the scattered frequency ω by requiring the phase of the scattered radiation to be continuous across the boundary at the trailing edge of the laser pulse [28], $\omega + v_g k = \omega_d + v_g k_d$, where $v_g = c(1 - \omega_p^2/\gamma_\perp \omega^2)^{1/2}$ and a square laser pulse profile has been assumed for simplicity. Using the dispersion relation to solve for k and k_d in terms of ω and ω_d , respectively, and assuming $\omega_p^2/\omega^2 \ll 1$, implies

$$\frac{\omega_d}{\omega} \simeq 1 + \frac{\omega_p^2}{4\omega^2} \left(1 - \frac{1}{\gamma_\perp}\right). \quad (83)$$

Hence, for backscattered radiation, the detected frequency will be upshifted from the scattered frequency. Furthermore, depletion of the electron plasma density within the region of the laser pulse by the transverse ponderomotive force will produce an additional upshift for similar reasons. This effect can be approximated by replacing $1/\gamma_\perp$ with $n_e/\gamma_\perp n_0$ in Eq. (83), where n_e/n_0 is given by Eq. (82). The maximum frequency upshift for the backscattered radiation can be estimated by $\Delta\omega_d/\omega \simeq \omega_p^2/4\omega^2$, which is typically small. Radiation scattered in the transverse or forward directions will not experience a frequency shift by these mechanisms.

VI. LASER SYNCHROTRON SOURCES

Nonlinear Thomson scattering can be used as a mechanism for generating x-ray radiation [1-9]. In such a laser synchrotron source (LSS), intense laser pulses are backscattered from a counterstreaming relativistic electron beam or from a dense plasma [5-7]. The LSS has the potential for providing a compact source of tunable, short pulse radiation, in the soft to hard x-ray regime. Two examples of LSS configurations will be discussed, one using a relativistic electron beam to generate hard x-rays (30 keV, 0.4 Å), and the other using a dense plasma to generate soft x-rays (300 eV, 40 Å). In the electron beam LSS, short wavelengths are generated by exploiting relativistic doppler factor, i.e., $\lambda = \lambda_0/4\gamma_0^2$, assuming $\gamma_0^2 \gg 1$ and $a_0^2 \ll 1$. In the plasma LSS short wavelengths are generated by exploiting the nonlinear harmonic factor, i.e., $\lambda = \lambda_0/n_c$, where $n_c \sim a_0^3 \gg 1$ is assumed. Both configurations will utilize the recently developed solid-state laser technology based on chirped-pulse amplification (CPA) [18-20]. Lasers based on CPA are relatively compact systems capable of delivering ultrahigh powers ($\gtrsim 10$ TW) and intensities ($\gtrsim 10^{18}$ W/cm²) in ultrashort pulses ($\lesssim 1$ ps). Currently, the repetition rates of TW CPA systems are limited to $\lesssim 10$ Hz [19,20]. A summary of the current state-of-the-art in CPA laser technology can be found in Ref. [20].

A. Electron-Beam LSS

An electron-beam LSS configuration consists of backscattering a linearly polarized laser pulse from a counterstreaming relativistic electron beam. Two important quantities characterizing the resulting synchrotron radiation are the photon flux, F , defined as the number of photons per second within a specified bandwidth, and the photon brightness, B , defined as the phase space density of the photon flux. The intensity distribution for backscattered, $\theta = 0$, radiation at the fundamental, $n = 1$, in the limit $a_0^2 \ll 1$ and $\gamma_0 \gg 1$ (i.e., $\omega \simeq \bar{\omega} = 4\gamma_0^2\omega_0$), is given by

$$\frac{d^2 I(0)}{d\omega d\Omega} = \frac{e^2 \omega^2}{8\pi c^2} \lambda_0 N_0 a_0^2 G_1(\omega), \quad G_1(\omega) = \frac{N_0}{\bar{\omega}} \left[\frac{\sin(\pi(\omega - \bar{\omega})N_0/\bar{\omega})}{\pi(\omega - \bar{\omega})N_0/\bar{\omega}} \right]^2, \quad (84)$$

as indicated by Eq. (39). The angular density of the flux, $dF/d\Omega$, i.e., the peak number of photons in a specified frequency range $\omega_1 \leq \omega \leq \omega_2$ emitted per second per unit solid angle

by the micropulse in the forward direction, can be determined from Eq. (84) by integrating over the frequency range $\Delta\omega_S = \omega_1 - \omega_2$, multiplying by the electron flux interacting with the laser, \dot{N}_b , and by dividing by the energy per photon, $\hbar\bar{\omega}$. The electron flux interacting with the laser field is given by $\dot{N}_b = fI_b/e$, where I_b is the peak micropulse current and f is the filling factor, i.e., $f = \sigma_0/\sigma_b$ for $\sigma_0 < \sigma_b$ and $f = 1$ for $\sigma_0 \geq \sigma_b$, where σ_0, σ_b are the cross-section areas of the laser and electron beam, respectively. The angular density of the flux is given by

$$\frac{dF_0}{d\Omega} = \alpha N_0 \dot{N}_b a_0^2 \gamma_0^2 \cdot \begin{cases} N_0 (\Delta\omega/\bar{\omega})_S, & \text{for } (\Delta\omega/\bar{\omega})_S \ll 1/N_0, \\ 1, & \text{for } (\Delta\omega/\bar{\omega})_S \gg 1/N_0, \end{cases} \quad (85)$$

where $\alpha = 1/137$ and F_0 denotes the spectral flux for an ideal electron beam, i.e., zero emittance and energy spread. For an ideal electron beam, the spectral flux with spectral width $(\Delta\omega/\bar{\omega})_S$ is given by $F_0 \simeq 2\pi\theta_R^2 (dF_0/d\Omega)$, where $\theta_R^2 = \theta_0^2 + \theta_S^2$, i.e.,

$$F_0 \simeq 2\pi\alpha N_0 \dot{N}_b a_0^2 (\Delta\omega/\bar{\omega})_S, \quad (86)$$

which is valid for all values of $(\Delta\omega/\bar{\omega})_S \leq 1$. For a realistic electron beam with finite emittance and energy spread, the photon flux, F , is identical to the ideal case, i.e., $F = F_0$. The angular density of the flux, $dF/d\Omega$, however, is reduced, since the photons are now spread out over a larger radiation angle θ_Σ , where θ_Σ is given by Eq. (79), i.e., $dF/d\Omega \simeq F_0/2\pi\theta_\Sigma^2$.

The spectral brightness is the phase space density of F . Hence, $B = F/(2\pi)^2 (R\theta_\Sigma)^2$, where $(R\theta_\Sigma)^2$ is the phase space area of the photon beam. The quantity R is the total effective size of the radiation source and is given by $R^2 \simeq r_s^2 + (\theta_\Sigma L/4\pi)^2$, where $\theta_\Sigma^2 = \theta_R^2 + \theta_i^2$, $\theta_i = (\Delta\omega/\bar{\omega})_i^{1/2}/\gamma_0$, and r_s is the smaller of r_b and $r_0/2$. Here L is the laser-electron interaction distance. The spectral flux and brightness for a non-ideal electron beam, in terms of practical units, are given by

$$F \left[\frac{\text{photons}}{\text{sec}} \right] = 8.4 \times 10^{16} f(L/Z_R) I_b [\text{A}] P_0 [\text{GW}] (\Delta\omega/\bar{\omega})_S, \quad (87a)$$

$$B \left[\frac{\text{photons}}{\text{sec} \cdot \text{mm}^2 \cdot \text{mrad}^2} \right] = 8.1 \times 10^9 f(L/Z_R) (I_b [\text{A}]/r_s^2 [\text{mm}]) \cdot E_b^2 [\text{MeV}] P_0 [\text{GW}] \left[\frac{(\Delta\omega/\bar{\omega})_S/(1+\delta)}{(\Delta\omega/\bar{\omega})_S + (\Delta\omega/\bar{\omega})_T} \right], \quad (87b)$$

where $\delta = (\theta_{\Sigma} L / 4\pi r_s)^2$ is typically $\ll 1$. The interaction length is the smaller of twice the Rayleigh length ($Z_R = \pi r_0^2 / \lambda_0$) or one-half the laser pulse length, i.e., $L = \min [2Z_R, L_0/2]$, unless it is further limited by the specific geometry of the experiment.

As an example, consider an electron beam LSS which generates 0.4 Å (30 keV) x-rays. For a $\lambda_0 = 1 \mu\text{m}$ incident laser, $\lambda = \lambda_0 / 4\gamma_0^2 = 0.4 \text{ \AA}$ implies $\gamma_0 = 79$ ($E_b = 40 \text{ MeV}$), assuming $a_0^2 \ll 1$. A CPA laser will be assumed with $\tau_0 = 2 \text{ ps}$, $P_0 = 10 \text{ TW}$ and $r_0 = 50 \mu\text{m}$, which implies $I_0 = 2.6 \times 10^{17} \text{ W/cm}^2$, $a_0 = 0.43$ and $Z_R = 7.9 \text{ mm}$. An electron beam from an rf linac will be assumed with peak current $I_b = 200 \text{ A}$, micropulse duration $L_b/c = 1 \text{ ps}$, beam radius $r_b = 50 \mu\text{m}$, energy spread $(\Delta E/E_b) = 0.5\%$ and normalized emittance $\epsilon_n = 5 \text{ mm-mrad}$. The interaction length is one half the laser pulse length, $L = 300 \mu\text{m}$, and the x-ray pulse duration is the micropulse duration, $\tau_x = 1 \text{ ps}$. The effective bandwidth is $(\Delta\omega/\bar{\omega})_T \simeq 1.4\%$ and this radiation is confined to a cone angle of $\theta_T \simeq 1.5 \text{ mrad}$. The total flux with $(\Delta\omega/\bar{\omega})_S \sim 1$ within the cone $\theta_c \sim 1/\gamma_0 \sim 12 \text{ mrad}$ is $F = 6.4 \times 10^{21} \text{ photons/sec}$. The peak brightness with $(\Delta\omega/\bar{\omega})_S = 0.1\%$ is $B = 2.9 \times 10^{19} \text{ photons/s-mm}^2\text{-mrad}^2$. The parameters for this electron beam LSS are summarized in Table I.

For simplicity, a counterstreaming laser-electron beam geometry has been assumed in which the x-ray pulse length is approximately the electron micropulse length. Shorter x-ray pulse lengths can be obtained by either reducing the laser Rayleigh length or changing the laser-electron beam intersection angle [6,8]. (Kim et al. [8] have suggested scattering at 90° to obtain ultrashort x-ray pulses.) In principle, both these methods may lead to the production of ultrashort x-ray pulses, with pulse durations on the order of the laser pulse duration.

B. Plasma LSS

To produce x-rays with a $\lambda_0 \sim 1 \mu\text{m}$ laser and a stationary plasma, it is necessary to use ultrahigh intensities, $a_0^2 \gg 1$. Nonlinear Thomson scattering will then occur in the asymptotic limit, in which a near continuum is produced with harmonics extending out to the critical harmonic number, $n_c \sim a_0^3$, as discussed in Section 2. Consider a linear polarized laser with $a_0^2 \gg 1$ interacting with a dense plasma. In the near backscattered

direction, the radiation spectrum scattered by a single electron is given by

$$\frac{d^2 I(0)}{d\omega d\Omega} = N_0 \frac{3e^2}{2\pi^2 c} a_0^2 Y(\xi), \quad (88)$$

as indicated by Eq. (75), where $Y = \xi^2 K_{2/3}^2(\xi)$, $\xi = \omega/\omega_c$, $\omega_c = n_c \omega_0$ and $n_c = 3a_0^2/4$. For a collection of electrons in a plasma, the total energy radiated is given by $E_T = N_e I(0)$, where $N_e = n_e \sigma_0 L_p$ is the total number of electrons with which the laser interacts, n_e is the plasma electron density, $\sigma_0 = \pi r_0^2/2$ is the laser cross-section and L_p is the laser-plasma interaction distance. Typically, $L_p \simeq 2Z_R = 2\pi r_0^2/\lambda_0$, assuming vacuum diffraction. The effects of relativistic optical guiding, however, could substantially increase the interaction distance [5,22,23,26,27]. Geometric arguments indicated that the x-ray pulse length in the backscattered direction is given by $L_x \simeq 2L_p(1 + L_0^2/4L_p^2)^{1/2} \simeq 2L_p$, where L_0 is the laser pulse length and $L_0^2/4L_p^2 \ll 1$ has been assumed. The total power in the backscattered direction is $P_T = cE_T/L_x$ and the photon flux is $F = P_T/\hbar\omega$. Hence, the flux intensity, defined to be $dF/d\Omega$, for photons in the frequency range $\Delta\omega_s$ about ω in the near backscattered direction, is given by

$$dF/d\Omega \simeq (3\alpha c/8\pi) N_0 n_e r_0^2 a_0^2 (\Delta\omega/\omega)_S Y(\omega/\omega_c). \quad (89)$$

Recall that the solid angle over which the photons with frequencies near ω_c are scattered is relatively large, i.e., $\theta_v \sim 2\sqrt{2}/a_0$ in the vertical direction and $\theta_h \sim \pi/2$ in the horizontal direction. The total photon flux, F , can be estimated by multiplying Eq. (89) by the appropriate solid angle over which the photons are to be collected. The brightness, B , of the backscattered photons can be estimated by $B \simeq (dF/d\Omega)/\pi r_0^2$. In practical units, the photon flux intensity and brightness are given by

$$\frac{dF}{d\Omega} \left[\frac{\text{photons}}{\text{s} \cdot \text{mrad}^2} \right] \simeq 3.65 \times 10^{-3} \tau_0 [\text{ps}] \lambda_0 [\mu\text{m}] n_e [\text{cm}^{-3}] P_0 [\text{TW}] \cdot (\Delta\omega/\omega)_S Y(\omega/\omega_c), \quad (90a)$$

$$B \left[\frac{\text{photons}}{\text{s} \cdot \text{mm}^2 \cdot \text{mrad}^2} \right] \simeq 1.80 \times 10^{-17} \tau_0 [\text{ps}] \lambda_0 [\mu\text{m}] n_e [\text{cm}^{-3}] I_0 [\text{W}/\text{cm}^2] \cdot (\Delta\omega/\omega)_S Y(\omega/\omega_c), \quad (90b)$$

As an example, consider a plasma LSS which generates 40 Å x-rays. For a $\lambda_0 = 1 \mu\text{m}$, $\tau_0 = 1 \text{ ps}$ incident laser pulse, $\lambda = \lambda_0/n_c = 40 \text{ Å}$ implies $n_c = 250$ and $a_0 = 6.9$, which

corresponds to a laser intensity of $I_0 = 6.6 \times 10^{19}$ W/cm². Assuming a laser spot size of $r_0 = 15$ μ m gives a laser power of $P_0 = 230$ TW and a laser-plasma interaction of length of $L_p \simeq 2Z_R = 1.4$ mm. The x-ray pulse duration is $\tau_x \simeq 2L_p/c = 9.4$ ps. A plasma density of $n_e = 10^{20}$ cm⁻³ implies a flux intensity of $dF/d\Omega \simeq 2.1 \times 10^{19}(\Delta\omega/\omega)_S$ photons/s-mrad² and a brightness of $B = 2.9 \times 10^{22}(\Delta\omega/\omega)_S$ photons/s-mm²-mrad². The parameters for this plasma LSS are summarized in Table II.

For simplicity, the generation of backscattered ($\theta = 0$) x-rays from the interaction of a linearly polarized laser and a plasma has been considered. For this case, the x-ray pulse length is of the order of a few Rayleigh lengths. However, Eqs. (36) and (46) indicate that somewhat larger fluxes of x-rays are emitted in the transverse direction ($\theta = \pi/2$) for both circularly and linearly polarized lasers incident on a plasma. Hence, by collimating the transverse emission from a plasma, ultrashort x-ray pulses can be obtained with durations, in principle, on the order of the laser pulse duration.

VII. CONCLUSION

A comprehensive theory describing the nonlinear Thomson scattering of intense laser fields from beams and plasmas has been presented. This theory is valid for linearly or circularly polarized incident laser fields of arbitrary intensities and for electrons of arbitrary energies. Explicit expressions for the intensity distributions of the scattered radiation were calculated analytically and evaluated numerically. The space-charge electrostatic potential, which is important in high density plasmas and prevents the axial drift of electrons, was included self-consistently. Various properties of the scattered radiation were examined, including the linewidth, angular distribution, and the behavior of the radiation spectra at ultrahigh intensities ($a_0^2 \gg 1$). Non-ideal effects, such as electron energy spread and beam emittance, which can broaden the linewidth and angular distribution of the scattered radiation, were discussed. These results were then applied to possible LSS configurations.

The general formula for the frequency of the Thomson backscattered ($\theta = 0$) radiation is given by $\omega_n = nM_0\omega_0$, where n is the harmonic number and M_0 is the doppler multiplication factor, given by Eq. (17). For a linearly polarized laser, only odd harmonics exist in the backscattered direction, whereas for circular polarization, only the fundamental is nonzero in the backscattered direction. Both odd and even harmonics can exist at off-axis angles. General expressions for the scattered intensity distributions are given by Eqs. (36) and (46). Generation of x-rays at short wavelengths require $M_0 \gg 1$ and/or $n \gg 1$. The intrinsic linewidth (i.e., for a cold electron distribution) of a particular harmonic is given by $\Delta\omega/\omega_n = 1/nN_0$, where N_0 is the number of laser periods with which the electrons interact. Since $N_0 \gtrsim 300$, small linewidths can be achieved. Non-ideal effects, such as energy spread and beam emittance, can broaden the linewidth, as indicated by Eq. (78). When $a_0^2 \ll 1$, radiation is scattered only at the fundamental. When $a_0^2 \gg 1$, a multitude of harmonics are produced, which results in a near-continuum of scattered radiation extending out to a critical harmonic number, $n_c \sim a_0^3$, beyond which the intensity of the radiation rapidly diminishes. Expressions for the scattered intensity distributions in the ultra-intense limit are given by Eqs. (69) and (75). The polarization of the scattered radiation can be adjusted by changing the polarization of the incident laser. Scattering from

an electron beam has the additional advantage of well-collimated radiation. For $\gamma_0 \gg 1$ and $a_0^2 \ll 1$, the upshifted radiation is confined to a cone about the backscattered direction of half-angle $\theta \simeq (\Delta\omega/\bar{\omega})^{1/2}/\gamma_0$. Scattering from a plasma has the advantage in the attainability of high electron densities, the photon flux and brightness scaling linearly with density.

A LSS, based on the nonlinear Thomson scattering of intense lasers from electron beams or plasmas, may provide a practical method for producing x-ray radiation. The LSS has a number of potentially unique and attractive features which may serve a variety of x-ray spectroscopic and imaging applications. These features include compactness, relatively low cost, tunability, narrow bandwidth, short pulse structure, high photon energy operation, well-collimated photon beams, polarization control, and high levels of photon flux and brightness. Specific examples of an electron-beam LSS and a plasma LSS were given, as summarized in Tables I and II. An electron-beam LSS, designed to generate 30 keV (0.4 Å) photons with a $\lambda_0 = 1 \mu\text{m}$ laser with $a_0 < 1$, requires a 40 MeV electron beam (approximately 300 times lower energy electrons than required by a conventional, storage-ring synchrotron). This electron beam LSS generates 1 ps x-ray pulses with a high peak flux ($\gtrsim 10^{21}$ photons/s) and brightness ($\gtrsim 10^{19}$ photons/s-mm²-mrad², 0.1%BW). A plasma LSS, designed to generate 40 Å (0.3 keV) photons with a $\lambda_0 = 1 \mu\text{m}$ laser, requires $a_0 = 6.9$ ($I_0 = 6.6 \times 10^{19}$ W/cm²). This plasma LSS generates < 10 ps x-ray pulses with a high peak flux ($\gtrsim 10^{21}$ photons/s, 10² mrad²) and brightness ($\gtrsim 10^{19}$ photons/s-mm²-mrad², 0.1%BW). These peak values of flux and brightness compare favorably to those obtained in conventional synchrotrons. High levels of average flux and brightness are presently limited by laser technology. The recent advances in compact, solid-state lasers, based on chirped-pulse amplification, are capable of generating the ultrahigh intensities ($a_0 \gtrsim 1$) needed to experimentally explore Thomson scattering and LSS x-ray generation in the nonlinear regime.

This paper has been restricted to the discussion and analysis of x-ray generation by the Thomson (incoherent) scattering of intense lasers from beams and plasmas. However, for sufficiently cold electron distributions, it is also possible to generate short-wavelength radiation by the stimulated (coherent) backscattering of intense lasers from beams and plas-

mas [5,21,29,30]. Stimulated backscattered harmonic generation may provided a method for producing coherent x-rays via a laser-pumped free electron laser (LPFEL). Advances in CPA lasers and in high-brightness electron beams may soon provide the necessary technology to realize compact sources of both incoherent (LSS) and coherent (LPFEL) x-rays.

Acknowledgments

The authors would like to acknowledge useful conversations with A. Ting, A. Fisher, and G. Mourou. This work supported by the Office of Naval Research, the Department of Energy, and the Medical Free Electron Laser Program.

References

1. E.S. Sarachik and G.T. Schappert, *Phys. Rev. D* **1**, 2738 (1970).
2. R.E. Waltz and O.P. Manley, *Phys. Fluids* **21**, 808 (1978).
3. P. Sprangle, B. Hafizi and F. Mako, *Appl. Phys. Lett.* **55**, 2559 (1989).
4. F. Carroll, J. Waters, R. Price, C. Brau, C. Roos, N. Tolk, D. Pickens and H. Stephens, *Investigative Radiology* **25**, 465 (1990).
5. P. Sprangle and E. Esarey, *Phys. Fluids B* **4**, 2241 (1992).
6. P. Sprangle, A. Ting, E. Esarey and A. Fisher, NRL Memo. Rep. 6973, Jul (1992); in *Proc. Workshop on 4th Generation Light Sources*, ed. by M. Cornacchia and H. Winick, Stanford Synchrotron Radiation Laboratory Report SSRL 92/02 (Stanford, CA, 1992), p. 280; *J. Appl. Phys.* **72**, 5032 (1992).
7. E. Esarey, P. Sprangle, A. Ting and S.K. Ride, accepted by *Nucl. Intr. and Meth.* (1993).
8. K.J. Kim, S. Chattopadhyay and C.V. Shank, submitted for publication.
9. C.I. Castillo-Herrera and T.W. Johnston, *IEEE Trans. Plasma Sci.* **PS-21**, 125 (1993).
10. K.J. Kim, in *Physics of Particle Accelerators*, edited by M. Month and M. Dienes, AIP Conf. Proc. 184 (Amer. Inst. Physics, New York, 1989), Vol. I, p. 565.
11. H. Winick, in *Physics of Particle Accelerators*, edited by M. Month and M. Dienes, AIP Conf. Proc. 184 (Amer. Inst. Physics, New York, 1989), Vol. II, p. 2138.
12. S. Krinsky, in *Proc. 1991 IEEE Particle Accelerator Conf.*, edited by M. Allen (IEEE, New York, 1991), Vol. I, p. 11.
13. A. Jackson, in *Proc. 1991 IEEE Particle Accelerator Conf.*, edited by M. Allen (IEEE, New York, 1991), Vol. IV, p. 2637.
14. B.M. Kincaid, *J. Appl. Phys.* **48**, 2684 (1977).
15. S.K. Ride and W.B. Colson, Stanford University High Energy Physics Lab Report 858 (1979).
16. R. Coisson, *IEEE J. Quantum Electron.* **QE-17**, 1409 (1981).
17. W.B. Colson, G. Dattoli and F. Ciocci, *Phys. Rev. A* **31**, 828 (1985).
18. D. Strickland and G. Mourou, *Opt. Commun.* **56**, 216 (1985); P. Maine, D. Strickland, P. Bado, M. Pessot and G. Mourou, *IEEE J. Quantum Electron.* **QE-24**, 398 (1988); M.D. Perry, F.G. Patterson and J. Weston, *Opt. Lett.* **15**, 1400 (1990); F.G. Patterson and M. Perry, *J. Opt. Soc. Am. B* **8**, 2384 (1991).
19. F. Salin, J. Squier and G. Vaillancourt, *Opt. Lett.* **16**, 1964 (1992).
20. G. Mourou and D. Umstadter, *Phys. Fluids B* **4**, 2315 (1992).
21. P. Sprangle and E. Esarey, *Phys. Rev. Lett.* **67**, 2021 (1991); E. Esarey and P. Sprangle, *Phys. Rev. A* **45**, 5872 (1992).
22. P. Sprangle, E. Esarey and A. Ting, *Phys. Rev. Lett.* **64**, 2011 (1990); *Phys. Rev. A* **41**, 4463 (1990); A. Ting, E. Esarey and P. Sprangle, *Phys. Fluids B* **2**, 1390 (1990).

23. P. Sprangle, E. Esarey, J. Krall and G. Joyce, *Phys. Rev. Lett.* **69**, 2200 (1992); E. Esarey, P. Sprangle, J. Krall, A. Ting and G. Joyce, *Phys. Fluids B*, July (1993).
24. J.D. Jackson, *Classical Electrodynamics*, second ed. (Wiley, New York, 1975), Chap. 14.
25. M. Abramowitz and I.A. Stegun, *Handbook of Mathematical Functions* (Dover, New York, 1970), p. 369.
26. G.Z. Sun, E. Ott, Y.C. Lee and P. Guzdar, *Phys. Fluids* **30**, 526 (1987); T. Kurki-Suonio, P.J. Morrison and T. Tajima, *Phys. Rev. A* **40**, 3230 (1989); P. Sprangle, A. Zigler and E. Esarey, *Appl. Phys. Lett.* **58**, 346 (1991); A.B. Borisov, A.V. Borovskiy, O.B. Shiryaev, V.V. Korobkin, A.M. Prokhorov, J.C. Solem, T.S. Luk, K. Boyer and C.K. Rhodes, *Phys. Rev. A* **45**, 5830 (1992).
27. C. Max, J. Arons and A. B. Langdon, *Phys. Rev. Lett.* **33**, 209 (1974); P. Sprangle, C.M. Tang and E. Esarey, *IEEE Trans. Plasma Sci.* **PS-15**, 145 (1987); W.B. Mori, C. Joshi, J.M. Dawson, D.W. Forslund and I.M. Kindel, *Phys. Rev. Lett.* **60**, 1298 (1988); E. Esarey, A. Ting and P. Sprangle, *Appl. Phys. Lett.* **53**, 1266 (1988).
28. C.B. Darrow, C. Coverdale, M.D. Perry, W.B. Mori, C. Clayton, K. Marsh and C. Joshi, *Phys. Rev. Lett.* **69**, 442 (1992).
29. R.H. Pantell, G. Soncini and H.E. Puthoff, *IEEE J. Quantum Electron.* **QE-4**, 905 (1968); A. Hasegawa, K. Mima, P. Sprangle, H.H. Szu and V.L. Granatstein, *Appl. Phys. Lett.* **29**, 542 (1976); P. Sprangle and A.T. Drobot, *J. Appl. Phys.* **50**, 2652 (1976); L.R. Elias, *Phys. Rev. Lett.* **42**, 977 (1979); T.M. Tran, B.G. Danly and J.S. Wurtele, *IEEE J. Quantum Electron.* **QE-23**, 1578 (1987).
30. P. Sprangle and E. Esarey, to be published.

Table I
Parameters for an Electron Beam LSS

Incident Laser Parameters

Wavelength, λ_0	1 μm
Pulse Length, L_0/c	2 ps
Peak Power, P_0	10 TW
Intensity, I_0	2.6×10^{17} W/cm ²
Strength Parameter, a_0	0.43
Spot size, r_0	50 μm
Rayleigh Length, Z_R	7.9 mm

Electron Pulse Parameters

Beam Energy, E_b	41 MeV
Beam Current, I_b	200 A
Beam Pulse Length, L_b/c	1 ps
Beam Radius, r_b	50 μm
Beam Energy Spread, $(\Delta E/E_b)_i$	0.5%
Beam Emittance, ϵ_n	5 mm-mrad

X-Ray Pulse Parameters

Photon Energy, E_p	30 keV
Photon Pulse Length, L_b/c	1 ps
Peak Photon Flux, ^a F	6.4×10^{21} photons/s
Photons/Pulse, ^a FL_b/c	6.4×10^9 photons/pulse
Peak Brightness (0.1% BW), B	2.9×10^{19} photons/s-mm ² -mrad ²
Angular Spread, $\theta_c \sim 1/\gamma$	12 mrad

^aIncludes all photons within the $\sim 1/\gamma$ angle, implying $\sim 100\%$ BW.

Table II
Parameters for a Plasma LSS

Incident Laser Parameters

Wavelength, λ_0	1 μm
Pulse Duration, τ_0	1 ps
Peak Power, P_0	230 TW
Peak Intensity, I_0	$6.6 \times 10^{19} \text{ W/cm}^2$
Strength Parameter, a_0	6.9
Spot size, r_0	15 μm
Rayleigh Length, Z_R	710 μm

Plasma Parameters

Electron Density, n_e	10^{20} cm^{-3}
Interaction Length, $2Z_R$	1.4 mm

X-Ray Pulse Parameters

Wavelength, λ_x	40 \AA
Photon Energy, E_p	310 eV
Photon Pulse Length, τ_x	9.4 ps
Flux Intensity (0.1% BW), $dF/d\Omega$	$2.1 \times 10^{16} \text{ photons/s-mrad}^2$
Brightness (0.1% BW), B	$2.9 \times 10^{19} \text{ photons/s-mm}^2\text{-mrad}^2$
Photon Flux ^a (100% BW), F	$6.5 \times 10^{21} \text{ photons/s}$

^aIncludes photons with $(\Delta\omega/\omega)_S \sim 1$ within a solid angle $d\Omega \sim \pi\theta^2$ with $\theta = 10 \text{ mrad}$.

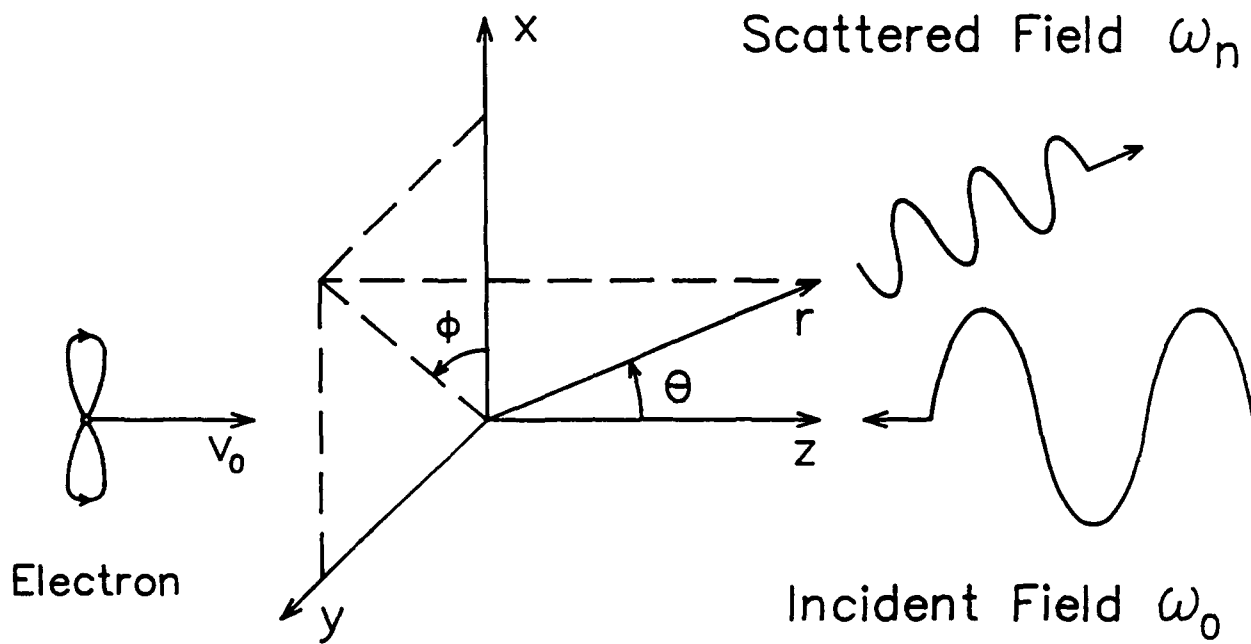


Fig. 1 Schematic diagram showing the Thomson scattering of an intense laser field from a free electron.

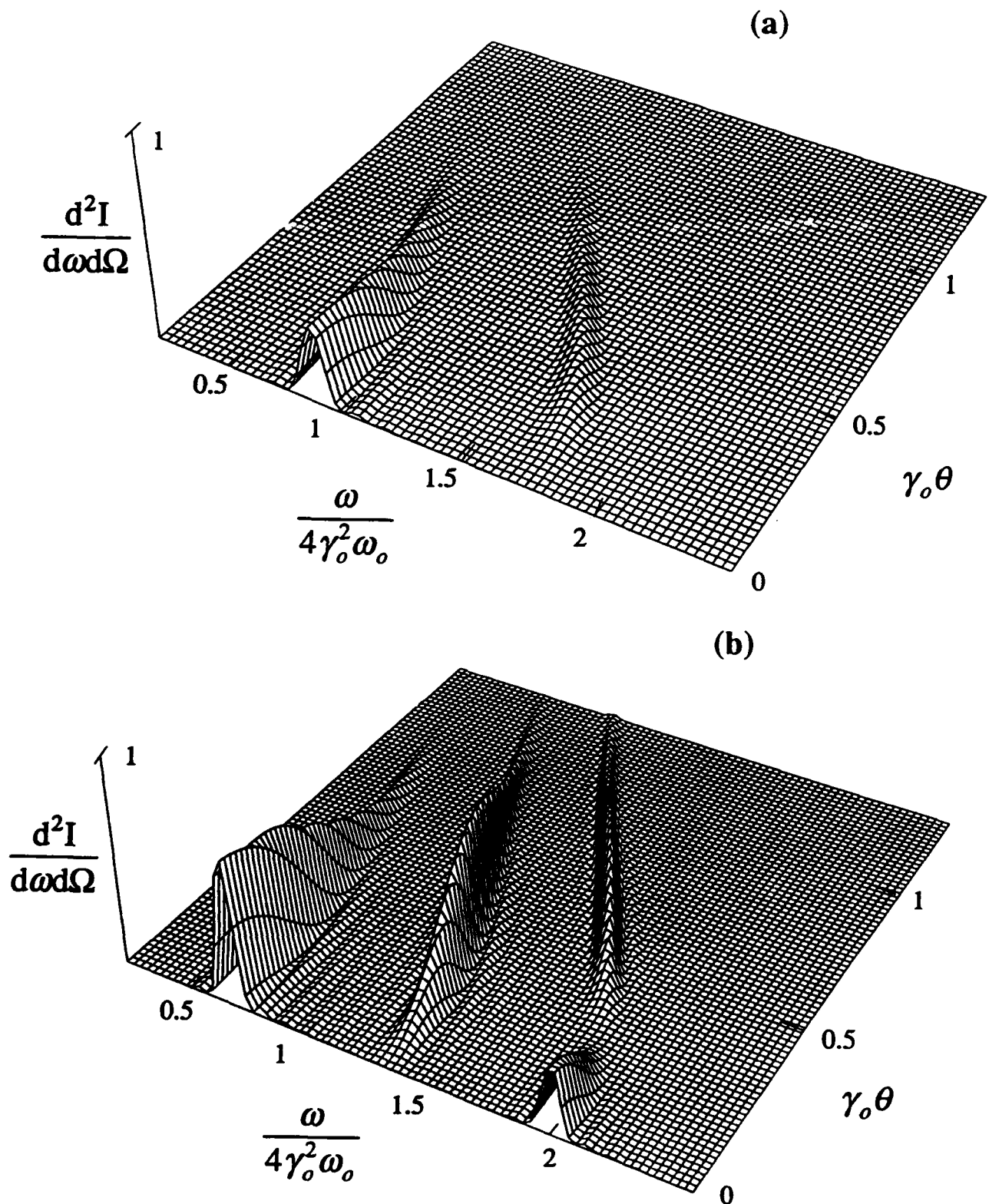


Fig. 2 The normalized intensity, as a function of normalized frequency, $\omega/4\gamma_0^2\omega_0$, and angle, $\gamma_0\theta$, in the $\phi = 0$ plane, of the radiation scattered by a relativistic electron ($\gamma_0 = 5$) from a counterpropagating, linearly polarized laser pulse ($N_0 = 7$). (a) shows the first two harmonics for $a_0 = 0.5$ and (b) shows the first three harmonics for $a_0 = 1.0$.

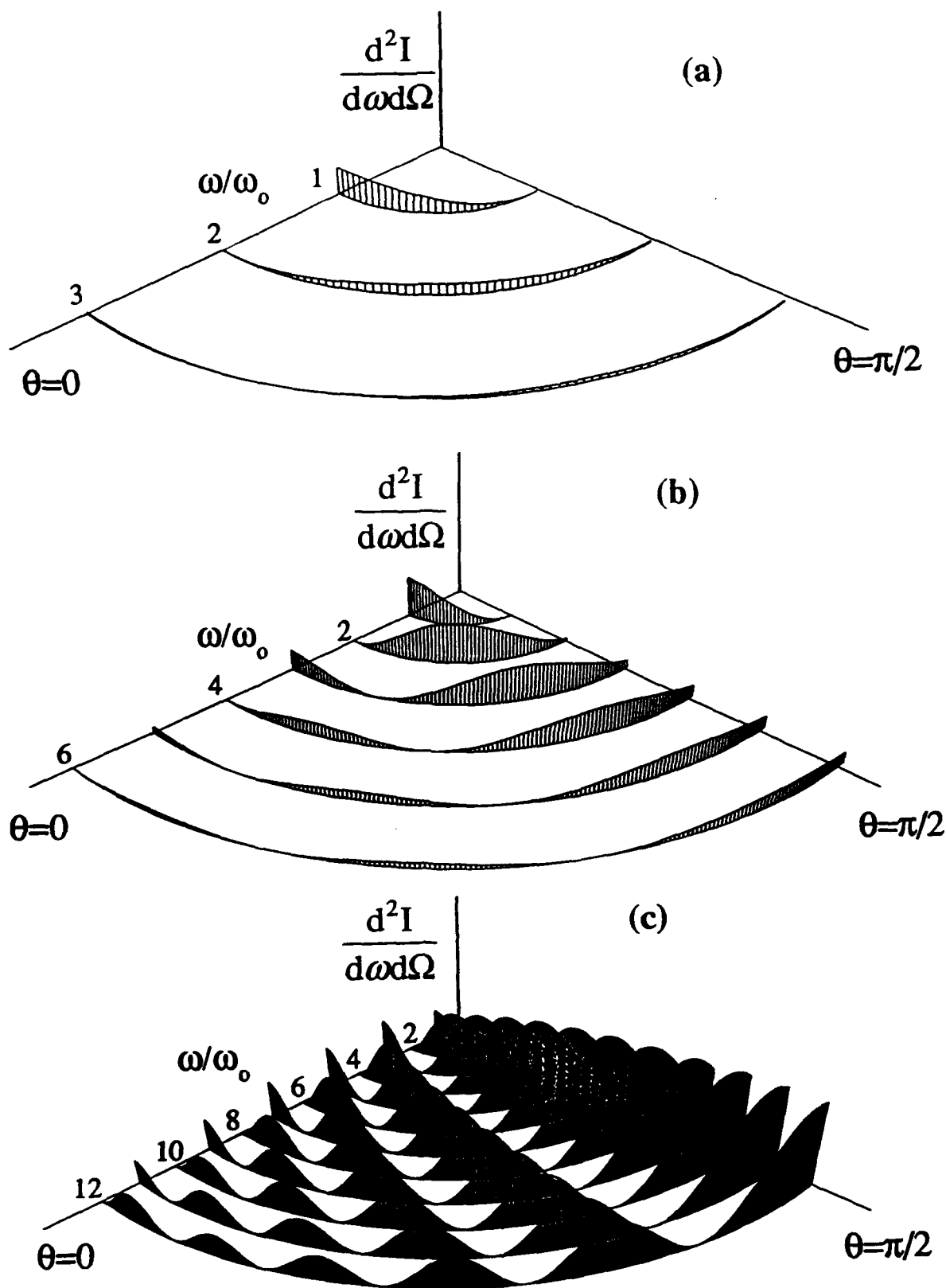


Fig. 3 The normalized intensity at the harmonic resonances, $\omega/\omega_0 = n$, as a function of angle, θ , in the $\phi = 0$ plane, of the radiation scattered by a dense plasma electron from a linearly polarized laser pulse ($N_0 = 7$). (a) shows the first three harmonics for $a_0 = 0.5$, (b) shows the first six harmonics for $a_0 = 1.0$, and (c) shows the first twelve harmonics for $a_0 = 2.0$.

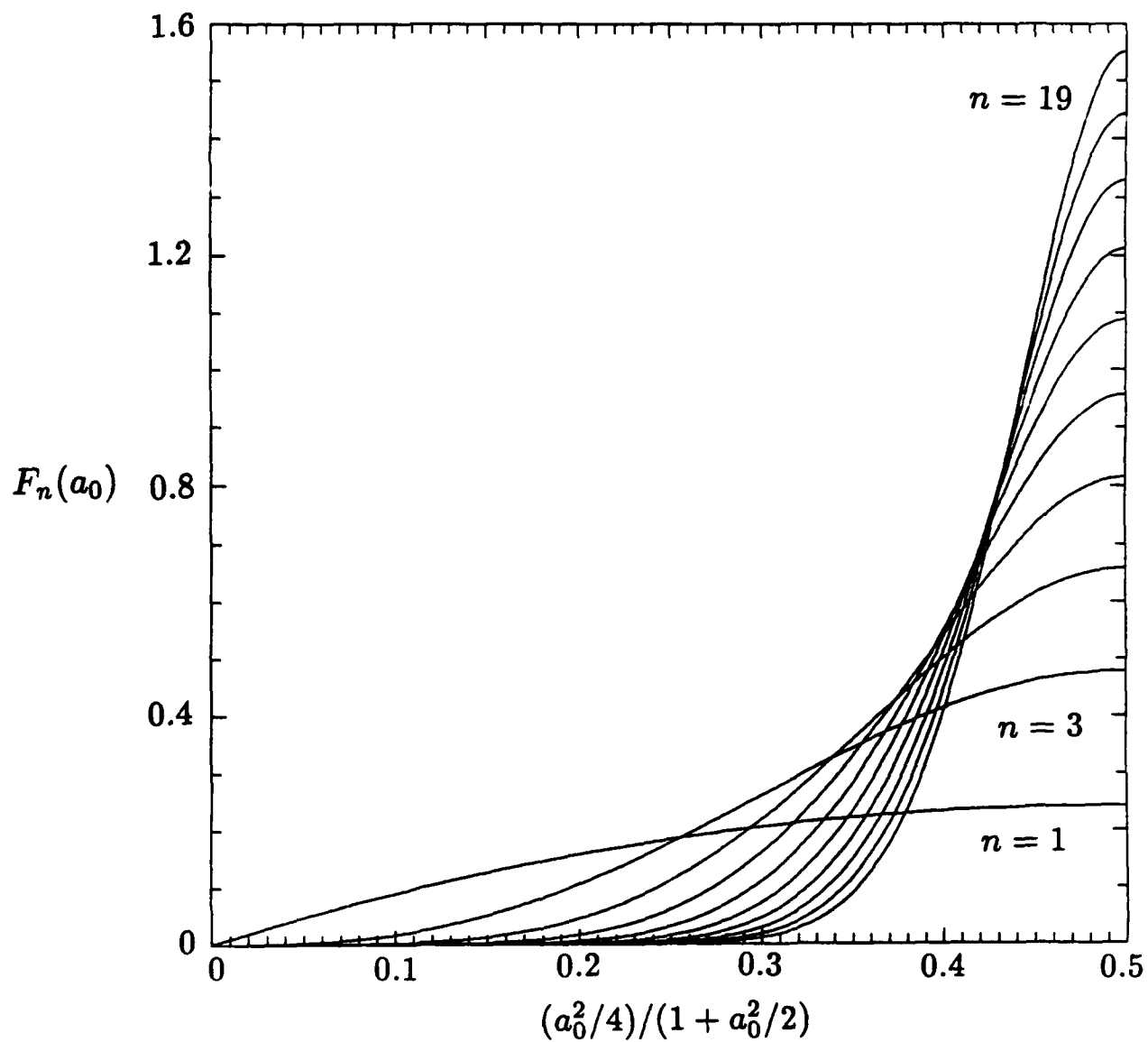


Fig. 4 The harmonic amplitude function, $F_n(a_0)$, as a function of $(a_0^2/4)/(1+a_0^2/2)$, for the first ten odd harmonics, $n = 1, 3, 5, \dots, 19$.

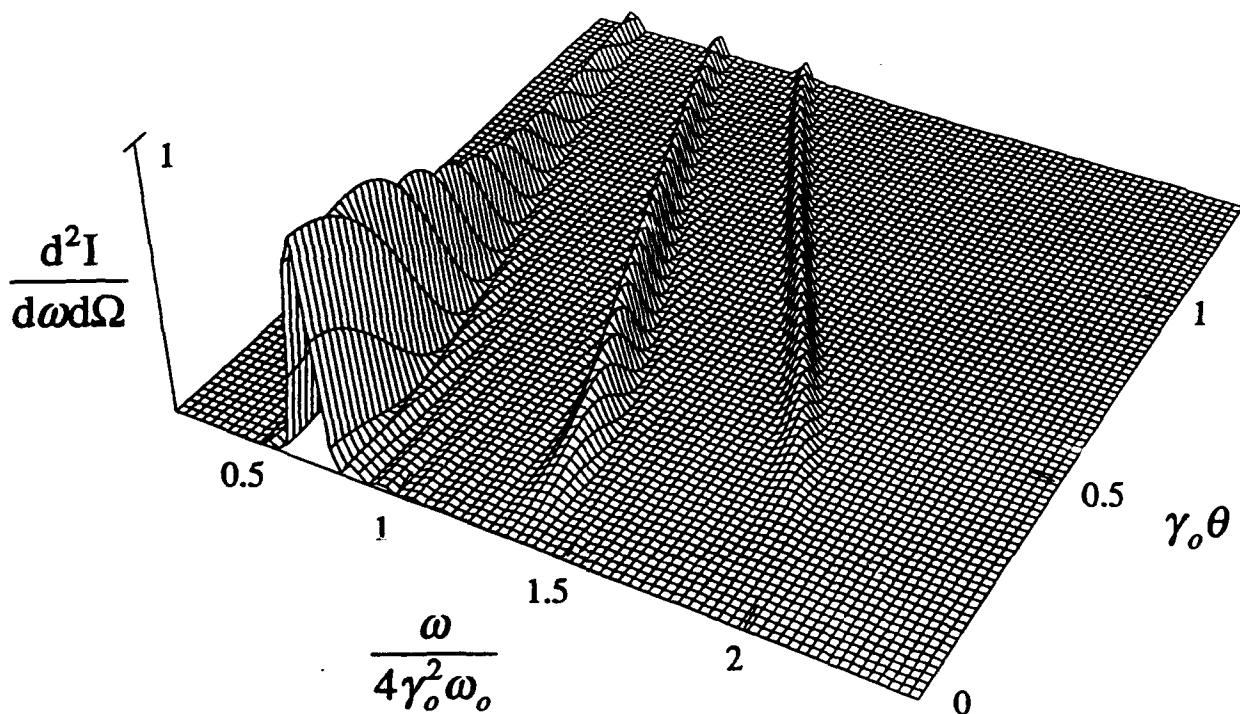


Fig. 5 The normalized intensity, as a function of normalized frequency, $\omega/4\gamma_0^2\omega_0$, and angle, $\gamma_0\theta$, of the radiation scattered by a relativistic electron ($\gamma_0 = 5$) from a counterpropagating, circularly polarized laser pulse ($N_0 = 7$, $a_0 = 1.0$) for the first three harmonics.

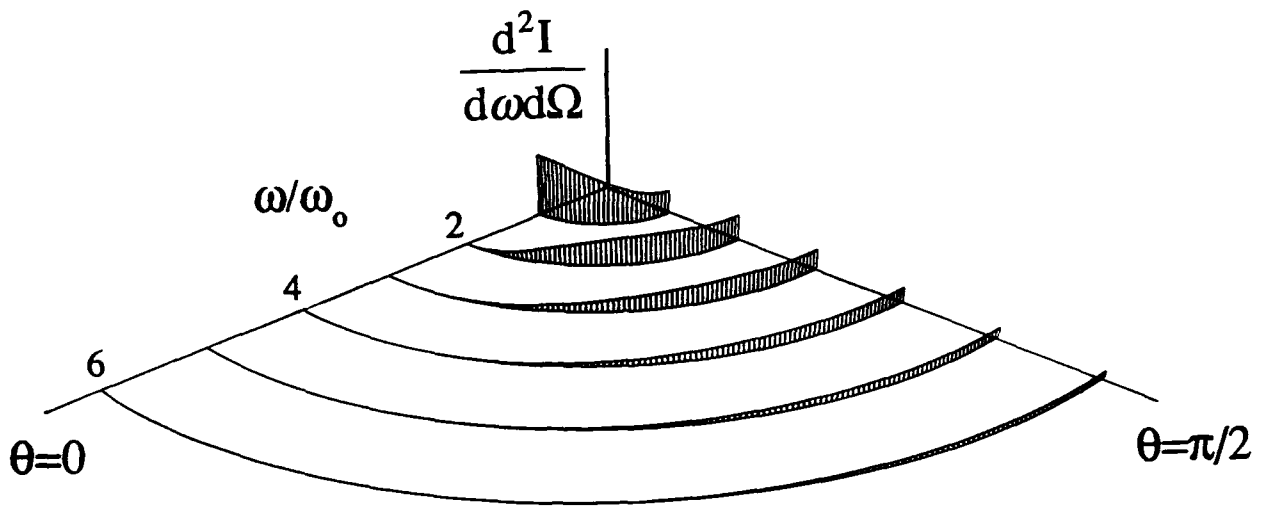


Fig. 6 The normalized intensity at the harmonic resonances, $\omega/\omega_0 = n$, as a function of angle, θ , of the radiation scattered by a dense plasma electron from a circularly polarized laser pulse ($N_0 = 7$, $a_0 = 1.0$) for the first six harmonics.

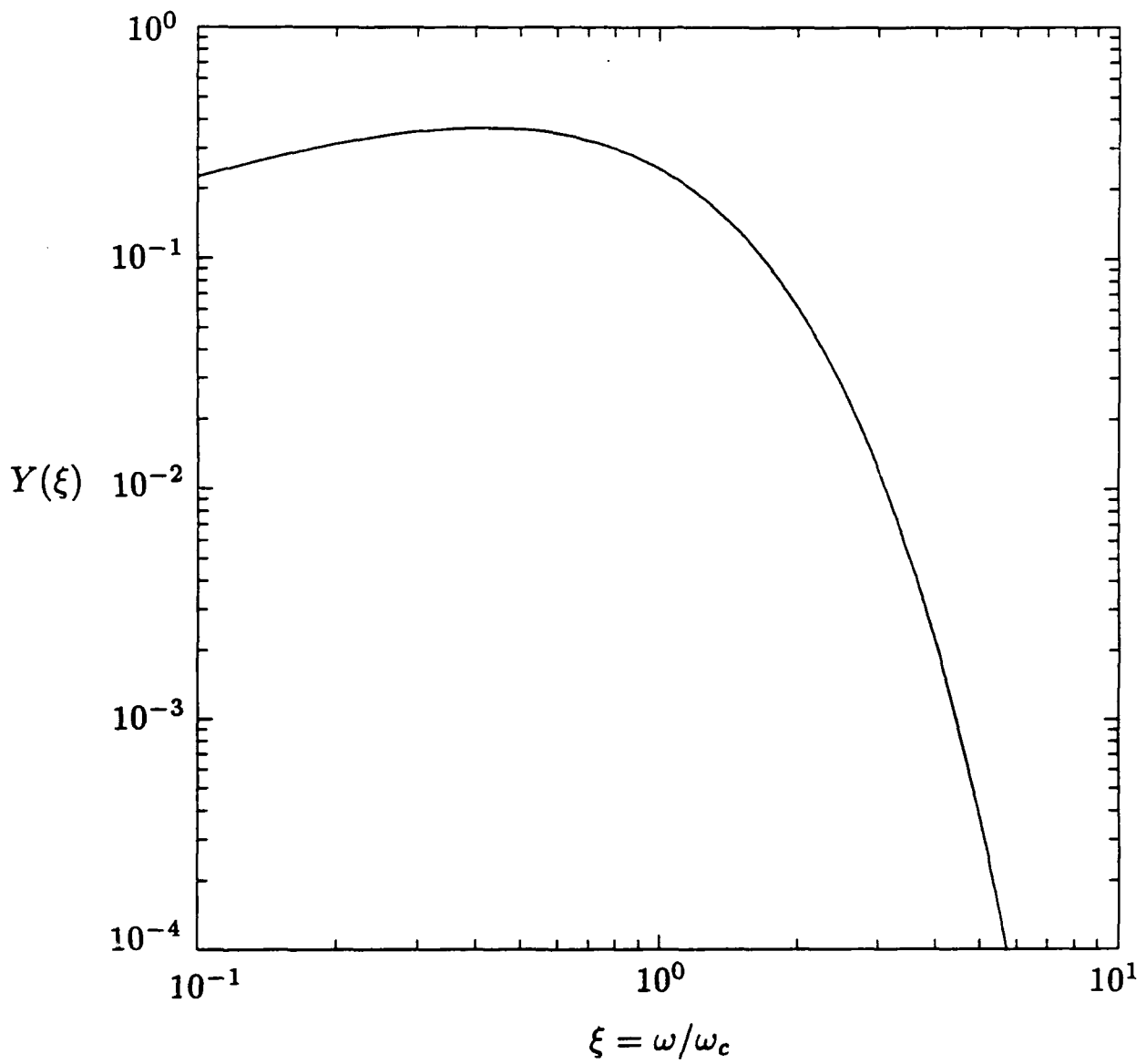


Fig. 7 The function $Y(\xi) = \xi^2 K_{2/3}^2(\xi)$ versus $\xi = \omega/\omega_c$.

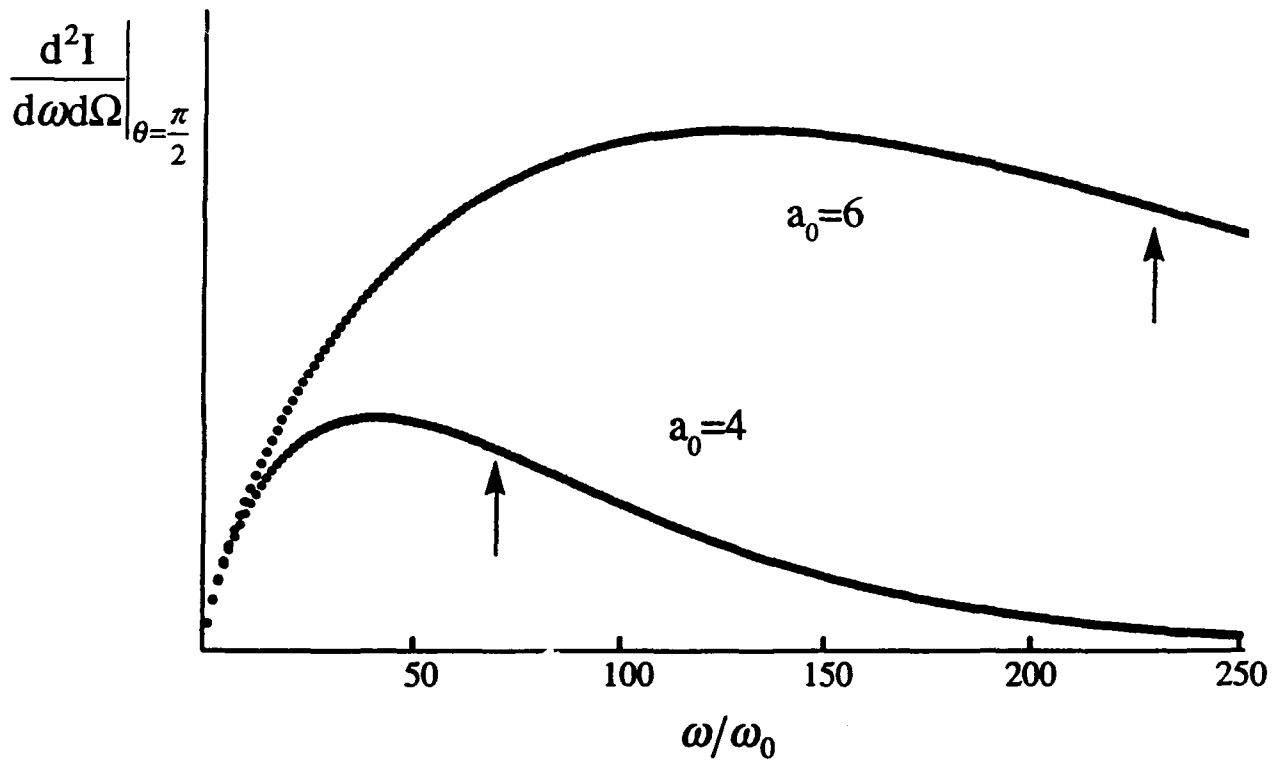


Fig. 8 The peak intensity of each harmonic in the transverse direction ($\theta = \pi/2$) versus normalized frequency, ω/ω_0 , for a circularly polarized laser scattering from a dense plasma electron. The cases $a_0 = 4$ and $a_0 = 6$ are shown. The arrows indicate the approximate critical harmonic number, $n_c \approx a_0^3$.

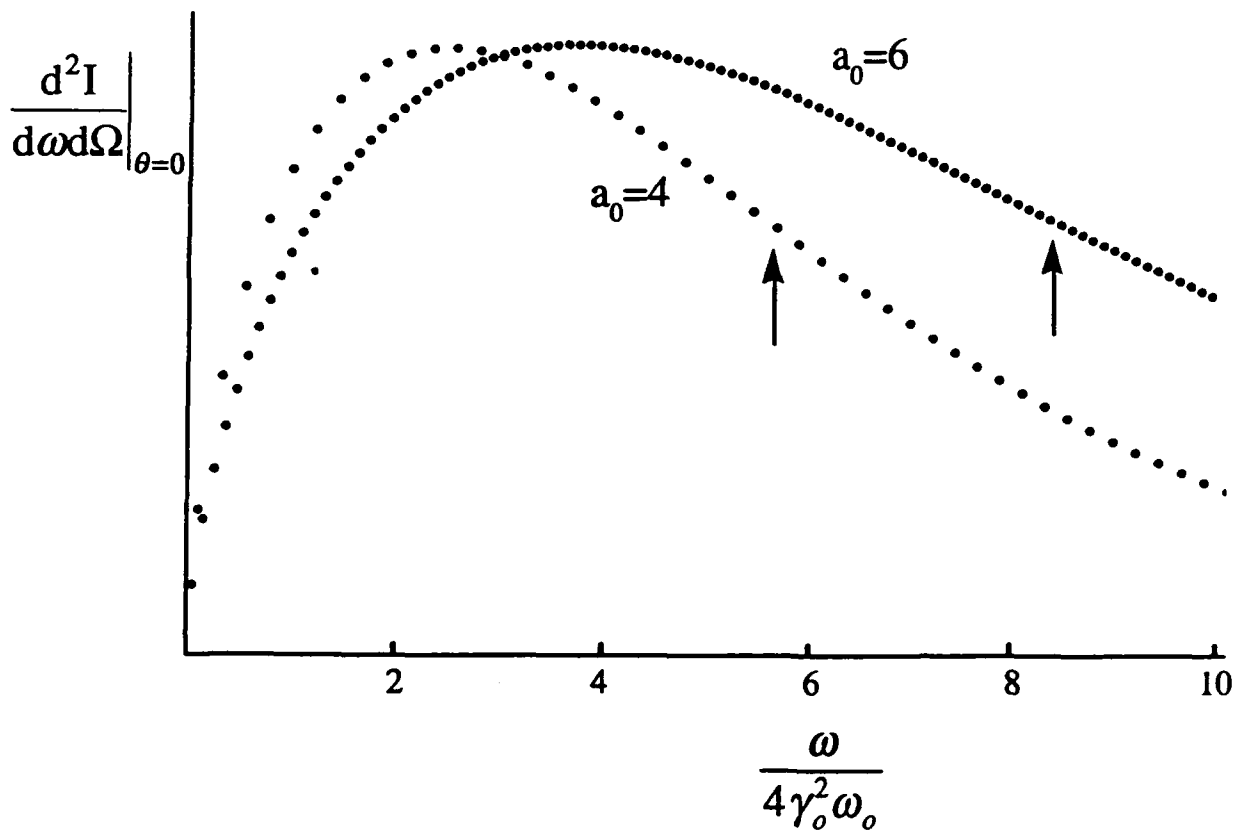


Fig. 9 The peak intensity of the odd harmonics on axis ($\theta = 0$) versus normalized frequency, $\omega/4\gamma_o^2\omega_o$, for a linearly polarized laser scattering from a counterstreaming relativistic electron ($\gamma_o = 5$). The cases $a_o = 4$ and $a_o = 6$ are shown. The arrows indicate the approximate critical harmonic number, $n_c \simeq 3a_o^3/4$.